# Doped graphene and curcumin@graphene composites for supercapacitance and electrochemical sensing applications

***A dissertation submitted in the partial fulfillment of the requirements for the degree of***

**MASTER OF SCIENCE**

in

**PHYSICS**

**Submitted By**

**Jaskiran kaur**

(Roll no: 302004014)


Under the guidance of

**Dr. Loveleen K. Brar**
**Assistant Professor**

**School of Physics and Materials Science**
**Thapar Institute of Engineering & Technology, Patiala-147004,**
**July-2023**

## Declaration

I hereby declare that the thesis titled **"Doped graphene and curcumin@graphene composites for supercapacitance and electrochemical sensing applications"** is the work carried out by me under the supervision of **Dr. Loveleen K. Brar** for partial fulfillment of the degree of Master of Science in Physics at School of Physics & Materials Science, Thapar Institute of Engineering and Technology, Patiala (Punjab), India. I have not submitted this work anywhere in other institutions for the award of any degree.

jaskiran kaur

**Jaskiran Kaur**

**(302004014)**

**Place:** Patiala

**Date:** 25-07-2023

## Certificate

This is to certify that the thesis titled **"Doped graphene and curcumin@graphene composites for supercapacitance and electrochemical sensing applications"** is an exclusive record of the candidate's research work done under me. To the best of my knowledge, this dissertation in part or full has not been submitted to any other institution for the award of any kind of degree.

**Dr. Loveleen K. Brar**
Assistant Professor
School of Physics and Materials Science
Thapar Institute of Engineering and Technology, Patiala

*Dedicated to*

*My Family*

*For their*

*love and*

*support*

## Acknowledgement

First of all, I bow my head in gratitude to GOD for his benign blessings and thank him for bestowing me the strength to complete this thesis.

With immense pleasure, I am thankful to my supervisor **Dr. Loveleen Kaur Brar**, School of Physics and Material Science (SPMS), Thapar Institute of Engineering & Technology (TIET), Patiala. Without her dedicated supervision, it would not have been possible for me to complete my thesis work. She always encouraged me whenever I felt down and motivated me to work harder. She was the one who motivated me to go for the work of my interest and every time I went to her with any kind of query, she was always there for me.

I would like to thank **Dr. O. P. Pandey** (Senior Professor), SPMS, for permitting me to use the facilities of his lab. Without his active support, it would have been not possible to carry out the experimental work.

I would like to express my sincere gratitude **to Dr. Kulvir Singh** (Head, SPMS) for his support and guidance and to all the members of the School of Physics and Materials Science for their help and suggestions at different stages of this work.

A special thanks to my lab mates **Mrs. Amanpreet Kaur, Mrs. Kaveri Ajravat,** and **Mrs. Raveena Choudhary** for the valuable suggestions, invaluable contribution, moral support, and guidance to enhance my working skills. During every difficult time in the research, I got motivation from them to deal with such challenges.

I am glad to thank my friends **Mr. Ashpreet Sharma**, **Ms. Amandeep Kaur (2), Ms. Amandeep Kaur (1), Ms. Komal Attri, Ms. Aditi Sharma and Mr. Shubham Sharma** for always motivating me to work harder and to move on with a positive spirit.

Last but not least, I place a deep sense of gratitude to my parents **Sh. Sukhwinder Singh & Smt. Kamaljeet Kaur** and younger brother **Mr. Gursewak Singh** for their sincere encouragement, and for being a source of inspiration throughout my thesis. Their blessings and love mean a lot to me and inspire me to pursue my work with full enthusiasm and great confidence.

**Jaskiran Kaur**

# Abstract

In this work, reduced graphene oxide (RG), sulphur-doped graphene (SG), and their respective composites with curcumin were synthesized and characterized for super capacitance and electrochemical $H_2O_2$ sensing applications. RG and SG were synthesized by a green one-pot hydrothermal method at a low temperature of 180º C. These samples were further used in oil bath heat treatment to synthesize the Curcumin@graphene composites. The morphological, and structural analysis of synthesized samples was done using Scanning Electron Microscopy, X-ray Diffraction, and Fourier Transform Infrared spectroscopy. Additionally, FTIR spectra offered valuable insights into the chemical functional groups and bonding characteristics of the materials. The SG electrode displayed a remarkable specific capacitance ($C_{sp}$) of 139.32 F/g at a scan rate of 3 mV/s, outperforming both RG and GO electrodes. The notable enhancement in capacitance can be attributed to the introduction of sulfur doping, which created abundant open-edge sites and defects within the graphitic frameworks. These structural modifications led to increased spin densities and the creation of more active sites for charge storage. Therefore, it was confirmed that sulfur doping of graphene-based electrode materials is an effective approach to improve their electrochemical performances. Curcumin@graphene composites were found to have enhanced the electrochemical performance. The SG-Cur composite showed excellent enhanced capacitance of 214.18 F/g at 3 mV/s and also had a higher ECSA value = 2021 as compared with SG (215.62) The strong interlinking between sulphur and curcumin within the composite enables efficient charge migration, resulting in higher electrochemical performance. Excellent hydrogen peroxide sensing performance was shown by the RG sample with 0.0069 μM limit of detection (LOD) in a 2-12 mM range. This excellent performance can be attributed to the high ESCA (1045.5) of the RG sample. The highly porous structure, chemical stability, and high specific surface area of the curcumin@graphene composite electrode are believed to be the reasons behind their excellent supercapacitance. Reduced sensing performance of Curcumin@graphene samples for $H_2O_2$ detection can be attributed to interlinking between curcumin and graphene-based samples resulting in decrease ECSA.

# List of Figures

# CHAPTER 1

# Introduction

## 1.1 Graphene Oxide

Graphene oxide (GO) is a two-dimensional nanosheet of highly oxidized carbon atoms with functional groups incorporating oxygen on its edges and basal plane as shown in Fig 1.1 [1]. It is a hexagonally organized planar sheet of carbon atoms, which is an allotrope of the element. GO is highly oxygenated, and in it the $sp^3$ hybridised carbon possesses hydroxyl and epoxy groups in addition to carbonyl and carboxyl groups that are present on the $sp^2$ hybridised carbon [2]. These functional groups contribute to GO's hydrophilic nature, making it easily dispersible in aqueous environments. GO has special characteristics such as high convective heat transfer, and low density.

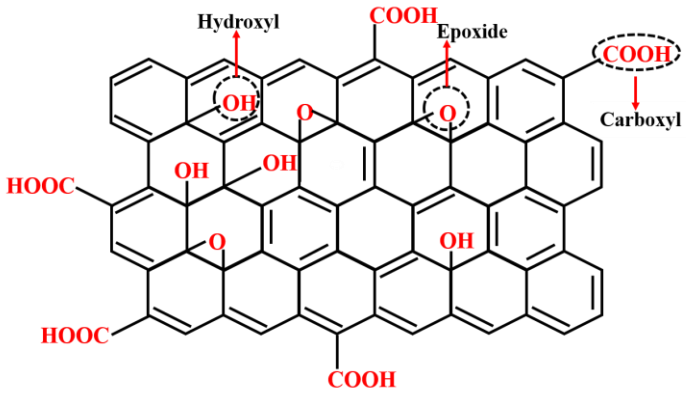


**Fig.1.1** Structure of graphene oxide.

GO can produce superior nano-composites due to its high oxygen content and surface area. This leads to better enhancement of mechanical and electrical properties for various applications [2]. Single-layer GO generally has a thickness of 0.7–1.2 nm. Numerous different techniques are being developed to create graphene oxide. One of the most widely used processes for producing GO is the modified Hummers technique [3]. It is a relatively simple and efficient method that produces

GO with a high degree of oxidation. It involves the sequential steps of oxidizing graphite and subsequently exfoliating it to obtain graphene oxide as shown in Fig.1.2.

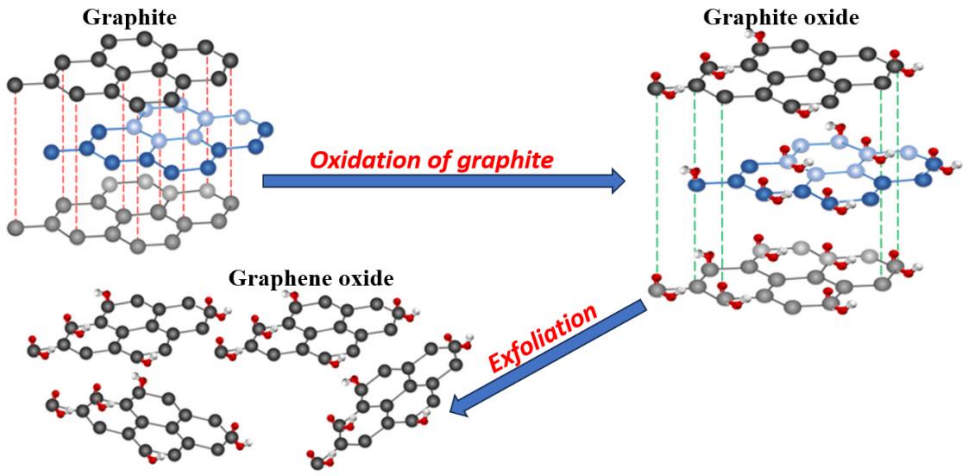


**Fig.1.2** Schematic of the GO synthesis process in modified hummer technique.

## 1.2 Properties of Graphene Oxide

- **Mechanical properties:** Young's modulus for the ordered graphene oxides is found to change by the coverage of the oxygen groups, going from 380 to 470 GPa. When considering amorphous graphene oxides with similar coverage, the variations in Young's modulus are relatively smaller, ranging from 290 to 430 GPa. Similar to the ordered graphene oxides, the amorphous ones have lower intrinsic strength. Young's modulus and intrinsic strength consistently decrease with increasing oxygen coverage as the $sp^2$ carbon network disintegrates and the energetic stability for both ordered and amorphous graphene oxides decreases [4].
- **Dispersibility:** Graphene oxide is readily exfoliated in water to produce a stable dispersion due to its hydrophilicity. Tetrahydrofuran (THF), ethylene glycol (EG), ethanol, and other organic solvents are a few examples of organic solvents in which the GO may disperse.
- **Electrical properties:** GO's electrical conductivity is lower than that of graphene, but it may be raised by lowering the oxygen level. This makes GO a promising material for applications where moderate electrical conductivity is required, such as sensors and batteries [4].

In comparison to graphene (G), GO offers the benefits of inexpensive manufacturing costs, mass production, and simple processing. It's a common first step in the production of graphene-based materials such as doped graphene and graphene composites, as well as reduced graphene oxide.

Reduced graphene oxide (RG) sheets demonstrate both enhanced chemical and physical adsorption capacity due to the abundant functional groups and strong electrical conductivity of its well-developed $sp^2$ networks. The applicability of single-component G is severely constrained by its limitations, which include poor electrochemical activity, easy agglomeration, zero band gap, and difficult processing [5]. The expansion of GO and RG's applications thus depends on functional modification.

## 1.3 Doped Graphene

Doping in graphene-based materials can be used to effectively modify their intrinsic and electronic characteristics, which can have a major impact on chemical processes at the interfaces and result in good electrochemical performance [6]. Doped graphene can be achieved through two methods: (1) substitutional doping, where heteroatoms replace carbon atoms in the graphene network, and (2) adsorption doping, where dopants are attached to the surface of graphene through adsorption processes. Substitutional doping exhibits higher stability compared to adsorption doping due to the covalent bonds that are created between the heteroatoms and the carbon lattice [7]. It enhances the electrochemical performance, chemical reactivity, and bandgap of graphene-based materials. Also, heteroatom doping gives additional pseudocapacitance, improves wettability, and also removes the restacking issue between the graphene sheets [8]. An increase in the band gap, the number of active sites, and the presence of $sp^3$ and $sp^2$ hybridization by doping graphene enhances its applicability. [7]. Phosphorus (P), sulphur (S), boron (B), and nitrogen (N) are the most common elements used to dope graphene because they have similar properties to carbon (C), such as size, electronic configuration, and number of valence electrons. The electronic configurations, sizes, valence electron numbers, and electronegativities of the dopant elements with carbon elements are contrasted in Table 1.1 [7].

Boron has a similar size (in terms of Van der Waals radius) and number of valence electrons (one less) to carbon, so it only causes minor changes to the lattice parameters of boron-doped graphene [7]. The slightly larger bond length for B-C bonds compared to C-C bonds can cause minor distortions in the planar structure of graphene at high doping levels. Nitrogen incorporation in graphene lattice distorts the planar structure of graphene at high doping levels, and the higher electronegativity of nitrogen can create a polarization in the carbon network. Due to its larger size compared to N, P-doping causes more structural damage in graphene, but P has a lower

electronegativity than C. Moreover, the doping effect of P is found to be different from that of N, due to the additional number of orbitals in P. Unlike the other dopants, sulfur has nearly same electronegativity to carbon, so it causes minor polarization of the C-S bonds. The longer bond length of the C-S bond compared to the C-C bond is typically what leads to the formation of defective sites in graphene upon S doping. [8][7].

**Table1.1** Comparison of different dopants.

| Element | Van der Waals radius (pm) | Electronic configuration | No. of valence electrons | Electronegativity |
|---|---|---|---|---|
| **N** | 155 | $1s^2 2s^2 2p^1$ | 5 | 3.04 |
| **B** | 180 | $1s^2 2s^2 2p^3$ | 3 | 2.04 |
| **S** | 180 | $1s^2 2s^2 2p^6 3s^2 3p^3$ | 6 | 2.58 |
| **P** | 195 | $1s^2 2s^2 2p^6 3s^2 3p^4$ | 5 | 2.19 |
| **C** | 170 | $1s^2 2s^2 2p^2$ | 4 | 2.55 |

## 1.4 Importance of Sulphur-Doped Graphene

Sulphur is the preferred choice among the heteroatoms for doping graphene because resulting materials are expected to have a wide band gap due to the electron withdrawing character of sulphur. It can also improve the wettability of graphene, which makes it more compatible with other materials. The high wettability of the surface of an electrode material reduces the resistance of ions to diffuse between the electrode and the electrolyte. The introduction of sulphur atoms in carbon materials increases the number of active sites on their surface, which enhances their catalytic ability and opens the band gap. This has led to the creation of sulfur-doped carbon materials for a number of applications, including the chemistry of fuel cells, semiconductor technology, sensors, supercapacitors, and more [9]. The distribution of non-uniform spin density on S-doped graphene is caused by a mismatch between the outermost orbitals of sulphur and carbon, which improves the catalytic characteristics suitable for various applications. Fig.1.3 shows the schematic for simultaneous reduction and doping of G by addition of $Na_2S$ [10].

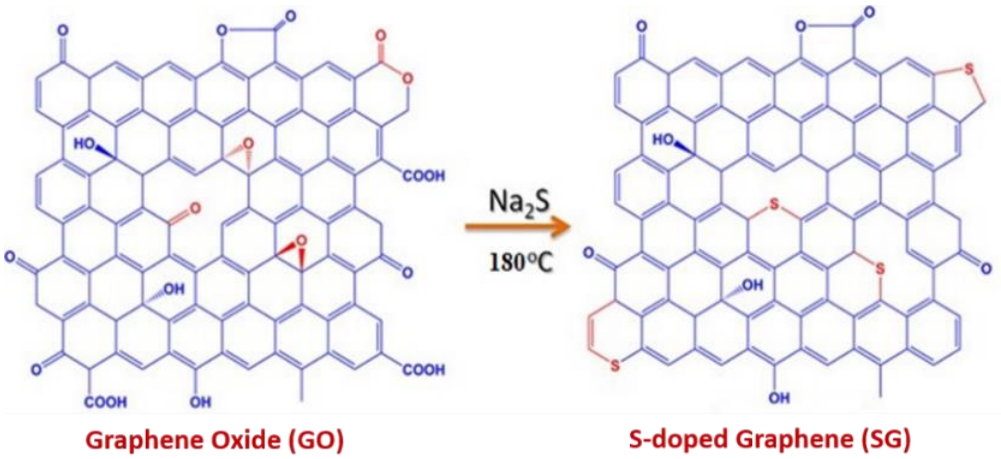


**Fig.1.3** Schematic of sulphur doping of graphene oxide using $Na_2S$.

## 1.5 Curcumin

Curcumin is a yellow-orange compound with a melting point of 183ºC with 368 g/mol molecular weight. Its solid form is 1,7-bis[4-hydroxy-3-methoxy phenyl]- 1,6-heptadiene-3,5-dione. It is a polyphenolic substance with two aromatic rings, each of which has a hydroxy and a methoxy substituent, as shown in Fig. 1.4 [11]. A seven-carbon chain with two tautomerizable-unsaturated carbonyl groups connects the rings. Although curcumin is soluble in ethanol and acetone, it is insoluble in water. About 5% bisdemethoxycurcumin, 15% desmethoxycurcumin, and 80% curcumin are naturally occurring curcuminoids in curcumin. It exhibits moderate instability in phosphate buffer at pH~7.4 and the stability is significantly increased by lowering the pH.

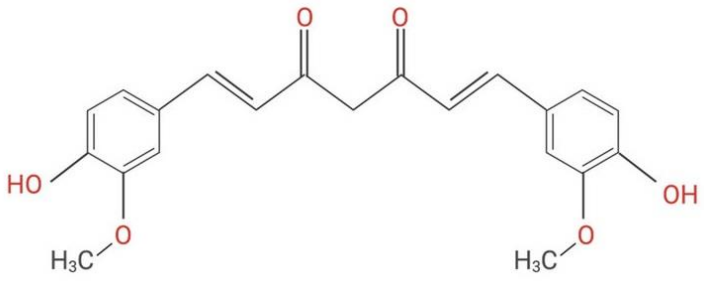

**Fig.1.4** Structure of curcumin

It has several potential applications, including as a dietary supplement, cosmetic ingredient, natural dye, and drug delivery system. The electrochemical efficiency of supercapacitors has been improved by the use of curcumin [12]. This is due to its ability to increase the electrode's capacitance and improves the electrolyte conductivity. curcumin has also improved the

electrochemical performance of reduced graphene oxide, sulfur-reduced graphene, and graphene oxide [13]. As a result, curcumin-modified graphene materials have potential uses in a range of electrochemical devices.

## 1.6 Supercapacitance and Electrochemical Sensing

Supercapacitors are a possible energy storage technology for the future since they offer high power densities and long cycle lifetimes. Supercapacitors may retain high power densities but have a poor energy density in comparison to other storage of energy devices like batteries, fuel cells, solar panels, etc. The lack of energy density limits applications that generally need to have significant energy as well as power density, such as hybrid automobiles [14]. The most important component for supercapacitors is generally considered to be the material of the electrode with high electrical conductivity, well-developed porosity, and high surface area [15]. The introduction of sulphur atom in graphene oxide and synthesis of graphene-based composites showed better super capacitive properties as reported recently. The advantage of electrochemical sensors over other types of sensors is that they can be easily miniaturized and offer wide detection limits, even for extremely small quantities of analyte. $H_2O_2$ is a typical oxidizing agent and an important intermediate that is widely used in clinical, biomedical, pharmaceutical, environmental, and many other domains. For this reason, it is crucial to develop quick, sensitive, and accurate $H_2O_2$ detection techniques [16]. In comparison to other $H_2O_2$ detection techniques like spectrophotometry, chemiluminescence, and fluorometry, the electrochemical technique has been viewed as the most promising approach due to its high sensitivity, good selectivity, and ease of use [17]. Doped graphene and graphene-based composites have been the subject of extensive research as efficient electrocatalysts to create electrochemical sensors and biosensors because of their superior electrical conductivity, sizable surface area, good biocompatibility, and simplicity of manufacture. RG is a highly appealing material due to its distinctive properties resulting from the presence of diverse functional groups. These functional groups contribute to enhanced selectivity and sensitivity for $H_2O_2$ detection [18]. The oxygen-containing groups present in RG play a vital role in its electrochemical performance, influencing factors such as electron transfer rate and the adsorption/desorption of molecules. Moreover, these oxygen-containing groups provide sites for anchoring enzymes or other species, making RG suitable for sensing [19].

# CHAPTER 2

# Literature Review

## Overview

The research and journal articles that were examined as part of the literature review are described in this section.

## 2.1 Synthesis of graphene oxide

**J. Chen et al 2013** [18] GO samples were synthesized by using Hummers method without (GO1) or with (GO2) using of $NaNO_3$. Graphite powder (3.0 g) was mixed with concentrated $H_2SO_4$ (70 mL) under stirring in an ice bath. $KMnO_4$ (9.0 g) was gradually added while maintaining the suspension's temperature below 20°C. The mixture was transferred to a 40°C oil bath, stirred for 0.5 h, and treated with water. Filtration, HCl washing, and air drying yielded solid GO. GO dispersion was obtained through exfoliation, centrifuged to remove unexfoliated graphite. The yields (the weight of GO divided by the weight of graphite powder) of GO1 and GO2 were measured to be 92% ± 3% and 96% ± 2%, respectively. This result indicates that the solution of concentrated $H_2SO_4$ containing $KMnO_4$ is capable of oxidizing graphite to GO in a yield close to that of Hummers method even without the assistance of $NaNO_3$.

**S.W. Chong et al 2015** [19] GO was synthesized using a simplified version of the Hummer's method. Around 3 g of graphite flakes were combined with 70 mL 0.5 M $H_2SO_4$ in an ice bath. Gradually adding 9 g $KMnO_4$, the mixture was stirred below 20°C to ensure safety. The temperature was raised to 35°C, stirred for 30 min, then heated to 95°C. Water and hydrogen peroxide were added, followed by washing with 1 M HCl, centrifugation, and further washing to eliminate metal ions. Reduction was performed using lemon juice, vinegar, and $N_2H_4$ as eco-friendly agents. This reduced GO exhibited a high electrical conductance of 24.6 µS attributed to its higher C/O ratio (~ 8:2) compared with other samples.

**N.I. Zaaba et al 2017** [20] GO was synthesized via a modified Hummers method from pristine graphite. A mixture of 27 ml sulfuric acid ($H_2SO_4$) and 3 ml phosphoric acid ($H_3PO_4$) (9:1 volume ratio) was stirred, with 0.225 g graphite added. Slow addition of 1.32 g potassium permanganate

($KMnO_4$) followed by 6 hours of stirring yielded a dark green solution. Excess $KMnO_4$ was reduced using 0.675 ml $H_2O_2$, then washed and centrifuged. The resulting GO solution was dried at 90°C for 24 hours, yielding GO powder.

**Q. Zhang et al 2022** [21] A modified method of manufacturing graphene oxide (GO) using boric acid ($H_3BO_3$) instead of sodium nitrate ($NaNO_3$) has been developed. In this, graphite powders (3.0 g), $H_3BO_3$ (3.0 g), and concentrated $H_2SO_4$ (120 ml) were introduced into a 500 ml flask, which was subjected to mechanical stirring at a rate of 200–250 rpm within an ice bath. Gradual addition of $KMnO_4$ (12.0 g) was carefully managed to maintain the suspension's temperature below 5 °C. The reaction setup was then moved to an environment of 20 ± 2 °C, where stirring at the same speed (200–250 rpm) was maintained for a duration of approximately 18 hours.

**X. Chen et al 2022** [22] Sodium nitrate (1 g) dissolved in 70 mL concentrated sulfuric acid. Flake graphite (2.0 g) stirred for 30 min at 0−4°C. Potassium permanganate (8.0 g) stirred 30 min. Temperature raised to 35−45°C, stirred 300 min. Deionized water (240 mL) added, stirred 120 min at 65−75°C. Hydrogen peroxide (25 mL, 30%) added, stirred 30 min at 95°C. Hydrochloric acid (40 mL, 5%) added, stirred 30 min. Vacuum extraction, hot filtration, washing, and centrifugation. GO solution pH adjusted (5−6), vacuum dried at 65°C to yield solid GO. This paper explains the chemical oxidation method's GO synthesis oxidizing reaction process.

**N. M. Lazano et al 2022** [23] GO was synthesized using a modified Hummers method omitting sodium nitrate ($NaNO_3$). Graphite (1 g) mixed with 23 mL sulfuric acid ($H_2SO_4$) stirred for 5 min in a cold bath. Potassium permanganate ($KMnO_4$) added, heated at 45°C for 2 h, then at 98°C with 46 mL distilled water for 15 min. Hydrogen peroxide ($H_2O_2$) and hot water (140 mL) added. Vacuum-filtered, washed with HCl and water by centrifugation. Dried at 60°C and 90°C for 24 h.

## 2.2 Synthesis of reduced graphene oxide and sulphur doped graphene by hydrothermal method.

**Y. Chen et al 2014** [9] S-GO was created by hydrothermally processing graphene oxide with $Na_2S$ as a precursor. First, 70 ml of DI was sonicated with 40 mg of graphene oxide to disperse it. Then 40 mg was added, followed by 15 minutes of stirring. The mixture was then heated to 120 to 180 degrees for 6 hours in an autoclave. The resulting S-GO contains 4.19at% sulphur and 4.73 at% oxygen.

**N. Cao et al 2015** [24] Hummers' liquid oxidation method was employed to synthesize graphite oxide from natural flake graphite. Subsequently, chemical reduction of graphene oxide was achieved using $NH_3$-$H_2O$ aqueous solution and hydrazine hydrate to produce reduced graphene oxide. The raw materials, namely graphite, graphite oxide, and reduced graphene oxide, were investigated utilising field emission scanning electron microscopy (FTIR) and X-ray diffraction (XRD).

**T. Zhengshan et al 2016** [10] prepared sulphur-doped graphene by using graphene oxide and as a $Na_2S$ precursor by hydrothermal reaction. Firstly, GO aqueous solution (3mg) was obtained by ultra-sonication in deionized water. Then a given amount was transferred into an 80 ml GO aqueous solution under magnetic stirring. The mixture was subsequently transferred to an autoclave and subjected to a 10-hour heating process at 200°C. The resulting sulfur content in SGO was determined to be 2.22 atomic percent (at%).

**Z.Zhian et al 2016** [25] Thioacetamide was used to prepare S-GO as a source of sulphur.0.3 g of thioacetamide powder was added to 40 ml of graphene oxide solution and stirred magnetically for 12 hours. The mixture was then placed into a stainless steel autoclave with a Teflon lining and heated to 185°C for 12 hours to speed up the reaction. The solution was then dried for 12 hours at 80 °C after being washed with deionized water three times.

**N. Raghavan et al 2018** [26] S-GO was created using graphene oxide as the initial component. Graphene oxide was used to prepare S-GO as a starting material. The sulphur was first dissolved in 2 ml of $CS_2$ solvent to create a homogeneous solution. The GO solution was then added to this mixture and sonicated for an hour. The solution was then placed in an autoclave and heated to 180 degrees for the following 18 hours. After that, the item was repeatedly rinsed in deionized water and dried for 12 hours at 80°C.

**A.S. Siddiqui et al 2019** [27] S-GO was created hydrothermally. GO was sonicated separately for 30 minutes before being combined with 50 mg of pluronic F-127. Then, 24.3 mg of sodium sulfide was added to the mixture and diluted to 150 ml. After being sonicated for an hour, the mixture was put in a 200 ml autoclave and heated to 180°C for the curse of seven hours. The product was collected after being washed in deionized water and dried for 24 hours at 45°C.

**D. J. Tarimo et al 2020** [28] synthesized S-RGO by mixing 1g of sulphur, 3 g of RGO, and 3 g of sodium sulfide into 100 ml of deionized water. The resulting mixture was then sonicated for 2 hours and transferred into stainless steel autoclave lined with Teflon for 12 hours at 180°C. The product was washed repeatedly with deionized water and then dried.

**M. Zhang et al 2021** [29] synthesized sulphur-doped graphene by using sodium thiosulphate ($Na_2S_2O_3$ ) as a precursor. In 50 ml of GO solution, 350 mg of $Na_2S_2O_3$ was added and ultrasonicated for 30 minutes. After that, the mixture was then heated to 220°C in an autoclave for 6 hours. The solution was then filtered, cleaned, and dried.

**N.H. Rosli et al 2021** [30] A microwave-assisted procedure with various $Na_2S$ concentrations was used to create sulfur-doped graphene (S-rGO). A mixture of 5 ml of 0.1 wt% GO and 5 ml of $Na_2S$ at concentrations of 0.15 M, 0.25 M, and 0.50 M was exposed to microwave-assisted reaction at 140 °C for 30 min, utilizing a Monowave 300 microwave reactor (Anton Paar). Following synthesis, the samples underwent three rounds of centrifugation at 12,000 rpm for 15 min. The resulting precipitate was collected and freeze-dried for a day. The enhanced supercapacitor performance of S-rGO was made possible by the pseudocapacitive properties of sulfur-containing groups.

## 2.3 Graphene composites with curcumin

**S. Hatamie et al 2015** [31] Curcumin was used to reduce GO sheets to functionalized curcumin-reduced graphene oxide sheets. The rGO sheets were found to be non-toxic to normal cells at concentrations less than 70 μg/mL. The rGO sheets induced apoptosis in cancer cells, which led researchers to conclude that they exhibited some cytotoxic effects at concentrations as high as 100 μg/mL. According to the study, curcumin-rGO shows promising potential as a therapeutic agent for cancer treatment.

**G. Elavarasi et al 2016** [32] The Hummers method synthesized graphene oxide (GO) from natural graphite. GO was combined with extracted curcumin to create Cur-GO. 5g of GO and 5 ml of curcumin are taken in Rb flask and dissolved in 50 ml of acetone and applied magnetics stirring for 20 hrs (1:2) ratio has been prepared by the same procedure. The structure of Cur-GO was characterized using IR and UV spectroscopy.The results obtained from this indicate that Cur-GO is more effective at inhibiting the growth of bacteria than GO alone.

F. Bugli et al 2018 [33] GO (Graphenea) in 2 ml dd$H_2O$ (2 mg ml-1) mixed with 2 ml curcumin (Sigma Aldrich) in ethanol (100, 200, 300 mg ml-1). Incubation at 70°C for 12 h, followed by adding 2 ml dd$H_2O$ to each sample, yielding 1 mg ml-1 GO. Centrifugation (15 min at 14,000 r.p.m.) performed twice to wash and remove unbound curcumin and ethanol. Notably, GOCU exhibits lower toxicity to cells compared to pure curcumin. Remarkably, it has shown effectiveness against MRSA at concentrations below 2 μg $ml^{-1}$. These findings strongly indicate the potential of GOCU as a promising treatment approach for MRSA infection.

**C.K. Das et al 2020** [34] Graphene-based materials, when combined with drugs, have been developed for cancer therapy. In this, graphene quantum dots (GQDs) and graphene were used just like carriers for curcumin (Cur) in different ratios. GO and GQDs dispersed in DI water (0.2 mg/mL), pH adjusted to 9.0 ± 0.1. Cur dissolved in DMSO (10 mg/mL), added to GO and GQDs at ratios 1:1, 1:3, and 1:5 (w/v) to create GO-Cur and GQDs-Cur derivatives. Homogenized, stirred 30 min at 4 °C, centrifuged (12,000 rpm, 20 min), pellet washed five times with DI water, vacuum dried.

**N. Nowroozi et al 2021** [35] Dispersion of GO was prepared through sonication by adding 4 milligrams of GO in one milliliter of DI water.1 ml of the GO suspension was slowly added drop by drop to a solution of dissolved curcumin (at a 3:1 Cur: GO ratio), which was then stirred for an hour. The mixture was then centrifuged for five minutes at 1000 rpm, followed by two washes in two ml of PBS to remove GO-trapped non-loaded curcumin particles.

## 2.4 Motivation

From the literature review, it is evident that there is a critical need to advance the development of high-performance energy storage systems and sensitive sensors for various technological applications. Graphene-based materials have shown immense potential in these domains, but further exploration of novel composites and their electrochemical performance is necessary. This thesis aims to address these gaps by proposing the synthesis of curcumin composites with reduced graphene and sulphur-doped graphene. The interaction of curcumin with the synthesized reduced and doped graphene samples will be investigated, focusing on the resulting changes in morphology and structure. The synthesis and characterization of curcumin@graphene composite materials will provide valuable insights for the development of advanced graphene-based materials with enhanced performance for energy storage and sensing devices.

# CHAPTER 3

# Materials and Methods

## Overview

In this chapter, the sample preparation methods and characterization techniques used in the current investigations are covered.

## 3.1 Materials

The materials used for the synthesis work were as follows:

1) **Graphite:** Graphite is a naturally occurring elemental mineral and is known as the crystalline form of carbon. As one of carbon's allotropes, it falls under the category of semi-metals. Graphite powder, <20µm, Avra Synthesis Pvt. Ltd.
2) **Sulphuric acid:** This substance, with the molecular formula $H_2SO_4$, is classified as a strong acid. It is characterized by its odorless, colorless, and viscous liquid state, readily soluble in water. In synthesis reactions, it exhibits highly exothermic behavior. $H_2SO_4$, 98%, Loba Chemie Pvt. Ltd.
3) **Phosphorus Pentaoxide:** It is a white solid that does not have any distinct odor. It has the chemical formula $P_2O_5$. When it comes into contact with water, it undergoes a highly exothermic hydrolysis reaction. $P_2O_5$, 98%, Loba Chemie Pvt. Ltd.
4) **Potassium Persulphate:** This inorganic compound has the chemical formula $K_2S_2O_8$. Known for its strong oxidizing properties, it is frequently used to initiate polymerization, leading to the formation of diverse C-N, C-S, C-O, and C-C bonds. The crystal structure of this compound is triclinic. $K_2S_2O_8$, 98%, Loba Chemie Pvt. Ltd.
5) **Potassium permanganate:** This chemical has the formula $KMnO_4$ and is an inorganic compound. It is a powerful oxidizing agent. It has a strong oxidizing effect. $KMnO_4$,99%, Loba Chemie Pvt. Ltd.
6) **Hydrogen peroxide:** It has a slightly higher viscosity than water and is a clear liquid. It serves as a bleaching and oxidizing agent. $H_2O_2$, 30% w/v, Loba Chemie Pvt. Ltd.
7) **Hydrochloric acid:** It is a powerful acid having distinctly powerful odour. HCL, 35% (extra pure), Loba Chemie Pvt. Ltd.

8) **Sodium sulphide:** The chemical compound with the formula $Na_2S$ is known as sodium sulfide. It is colorless and when dissolved in water gives a strongly alkaline solution. $Na_2S$, SD fine-chem Ltd.
9) **Curcumin:** Curcumin is a component found in turmeric and is categorized as a curcuminoid, also referred to as diferuloylmethane. The chemical name for it is 1,7-bis [4-hydroxy 3-methoxy phenyl]- 1,6-heptadiene-3,5-dione. In organic solvents, it exists in an enolic form, while in water, it takes on a keto form. $C_{21}H_{20}O_6$, Central Drug House (P) Ltd.

## 3.2 Synthesis Methods

The synthesis experiments were performed by employing the following methods:

### 3.2.1 Graphene oxide

Graphite powder was used as the starting material for the two-step, modified Hummers method of producing graphene oxide (GO). In the first step, graphite powder was dispersed in concentrated $H_2SO_4$ along with equal amounts of $P_2O_5$ and $K_2S_2O_8$. For 4.5 hours, the mixture was stirred at 80°C. After adding 320 ml of deionized (DI) water, the finished product was washed and dried at 80°C. In the subsequent step, concentrated $H_2SO_4$ (80 ml) and preoxidized graphite powder were combined. For 2.5 hours, stirring was done while adding $KMnO_4$ (10 g) gradually. The mixture was then stirred for an additional two hours after DI water was added. Before washing with HCl (10%) and DI water, diluted $H_2O_2$ was added. At 80°C, the finished product was dried.

### 3.2.2 Sulphur-doped graphene/ reduced graphene oxide

Sulphur-doped graphene (SG) was synthesized by the direct hydrothermal treatment of GO and $Na_2S$ as a precursor in a Teflon-lined stainless-steel autoclave. The as-synthesized graphene oxide (GO) dispersion, with a concentration of 1.4 mg/ml, was utilized to synthesize the SG sample through the addition of $Na_2S$. The required precursor was mixed with 20 ml of GO dispersion using ultrasonification for 40 minutes. Subsequently, the material was subjected to hydrothermal treatment in an autoclave lined with Teflon at a temperature of 180°C for 12 hours. After the hydrothermal treatment, the product was washed with deionized (DI) water and dried overnight at 80°C. The resulting final product was then collected. For comparison, RG was prepared without the addition of $Na_2S$ precursor under the same conditions as those for the SG sample.

### 3.2.3 Synthesis of curcumin@graphene composites

5 mg of curcumin was dissolved in 1 mg/ml of ethanol and then combined with 2 mg/ml of GO in 5 ml of DI water while being stirred. Then, while stirring for 2 hours at 85° C, ammonia was added to the Cur-GO suspension to raise the pH~10. The finished product was then collected after being washed with DI water and allowed to dry for an entire night at 80° C. Similarly, SG and RG composites with curcumin are synthesized under the same conditions as those for curcumin@graphene composites.

## 3.3 Characterization Techniques

### 3.3.1 X-Ray Diffraction

X-Ray Diffraction (XRD) is a non-destructive technique for atomic spacing, phase examination, and crystal structure. It is used for determining the interplanar spacing between the materials' stacked layers. The basis of this technique is based on the homochromatic X-rays' constructive interference. A cathode ray tube (CRT) is used to generate X-rays for this technique. The CRT acts as a filter, producing monochromatic radiation. The sample which needs to be examined is then focused by this radiation. The relationship between the constructive interference of rays is established by Bragg's law, which is given by:

$$2d \sin \theta = n \lambda \tag{3.1}$$

Where n can be any positive integer, d is the distance between diffracting planes, $\theta$ the angle of incidence, and $\lambda$ =1.54 Å (X-ray wavelength) . XRD is a very significant method to comprehend the number of layers, crystalline structure, and interplanar spacing of graphene oxide & reduced graphene oxide. So, it is a technique for characterization that is usually used. Graphene's layers are separated by a distance(d) which may be determined using Bragg's equation (3.1). Equation 3.2 is employed to determine the average height of stacking layers of graphene oxide, denoted as H, with a constant of 0.9 applied to the (002) reflection. To figure out the average diameter of stacking layers denoted as D, Scherrer's equation is applied to a two-dimensional (10) reflection [36]. The Pearson seven fitting is used to obtain the full width at half maximum (FWHM) values from X-ray diffraction data. Scherrer’s equation:

$$\tau = K \lambda / \beta \, \mathrm{Cos} \, \theta \tag{3.2}$$

where: τ = crystalline size, K is a constant with a dimensionless value of 0.9, for 3-D reflection and 1.84 for 2-D reflection, β = FWHM, and θ = Bragg angle.

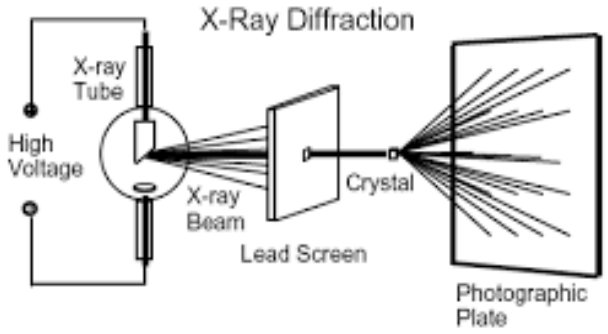


**Fig.3.1** Systematic image of XRD

The step size for the XRD pattern was 0.013, and the 2θ values were taken in the 5˚ to 90˚ range.

### 3.3.2 Fourier-transform infrared spectroscopy (FTIR)

The FTIR spectrum is an analytical tool used to determine the functional groups of a specific compound and assess the sample's purity. It involves measuring how much of various frequencies are absorbed by a sample that has been placed in an IR beam's path. It offers a spectrum with many absorption bands and information on the structure of a specific compound [37].

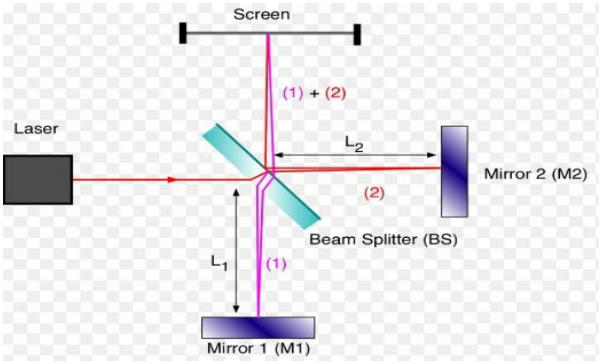


**Fig.3.2** Internal Diagram of FTIR

The IR spectrum is typically displayed using the wave number on the x-axis and the percent transmittance on the y-axis. The range of measurements was 500cm$^{-1}$ to 4000cm$^{-1.}$

### 3.3.3 Scanning Electron Microscopy (SEM)

A focused electron beam is used by the potent imaging method known as scanning electron microscopy (SEM) to produce high-resolution pictures of surfaces and structures. SEM works on the fundamental aspect that a sample surface is scanned with an electron beam, and the secondary electrons that are emitted from the surface are then detected. The surface morphology is then precisely pictured using these secondary electrons. SEM images have a deeper field of view, giving them a three-dimensional look that helps to better understand the sample's surface characteristics.

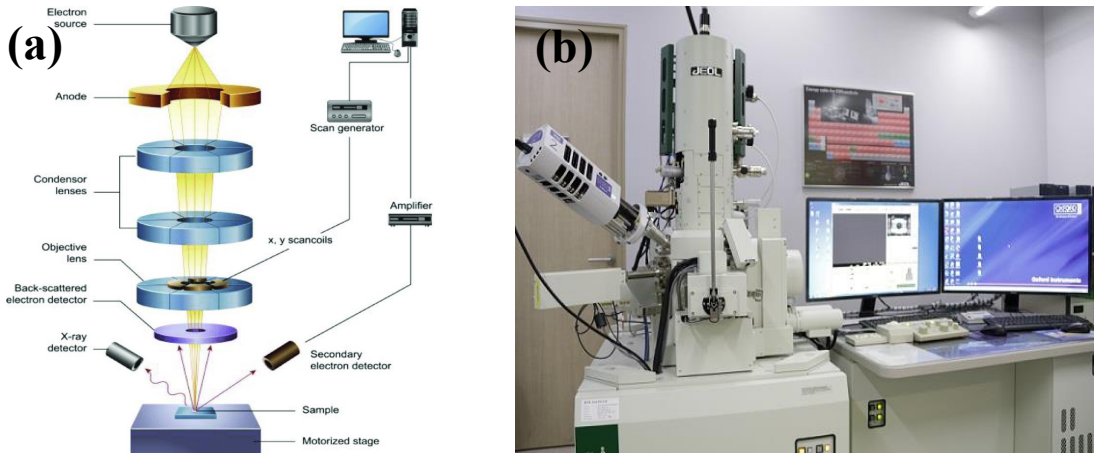


**Fig.3.3** (a) Schematic for SEM device (b) Laboratory view of SEM device

It can produce images with a lot higher resolution than conventional light microscopy, enabling the visualization of surface features as small as a few nanometers. SEM is frequently used in biology, materials science, and other disciplines to examine the morphology, structure, and makeup of different samples [38]. Fig.3.3(a) shows the schematic diagram of the SEM.

### 3.3.4 Energy dispersive spectroscopy (EDS)

It is a technique to find out the elements of any sample. Each element has a different atomic structure, which results in a different set of peaks on its electromagnetic emission spectrum. X-rays or high-energy electron beam is used for EDS. EDS measures the energy of X-rays coming from the sample. This energy represents the atomic structure of the element and the distinction between the two shells. A brass stub was used to prepare the sample. To completely remove the sample’s moisture, it was placed on the stub and completely dried under a lamp.

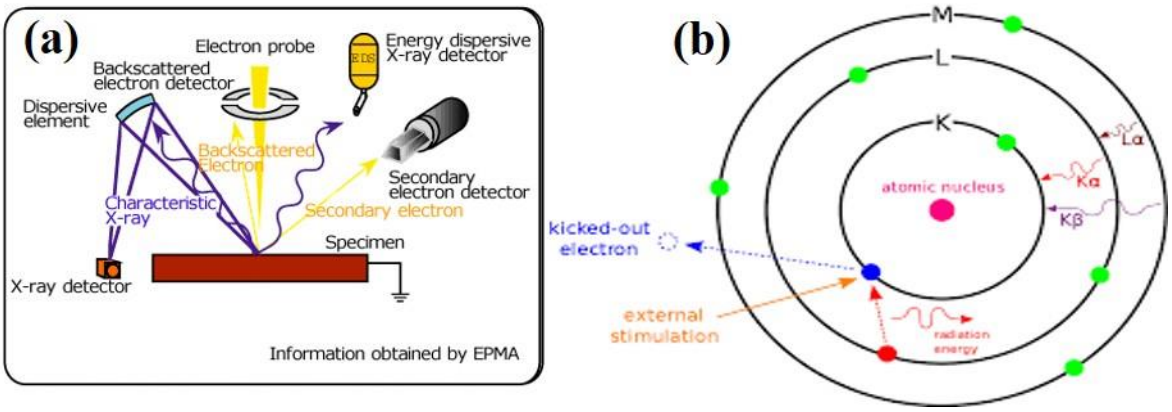


**Fig.3.4** (a) Schematic of EDS, (b) Diagram showing the principle of EDS

A gold coating was applied to the sample after that, and an EDX analysis was performed to determine the elemental composition. The principle of EDS is shown in Fig. 3.4(b)

### 3.3.5 Supercapacitor measurement

To investigate the capacitance performance of the synthesized samples in an acidic medium, a Bio-Logic EC Lab SP300 with a typical three-electrode configuration was used. Saturated calomel electrode (SCE) functions as the reference electrode, and platinum wire acts as the counter electrode. The working electrode is a glassy carbon electrode (GCE) that has been loaded with a sample. For the tests, these were immersed in a solution of 1 M $H_2SO_4$ as an electrolyte.

Before the measurement, the working electrode which was loaded with the sample underwent pretreatment with potential cycling between -0.15 V and +1.15 V (80 cycles at a sweep rate of 80 mV/s) to activate the catalyst, remove surface impurities and stabilize the electrochemical current. A potential window of 1.2 V, ranging from -0.1 V to 1.1 V, was used for the cyclic voltammetry (CV) measurements to evaluate the electrochemical capacitance. The scan rates used for these measurements varied from 3 to 220 mV/s. Galvanostatic charge-discharge (GCD) curves were also obtained using a 1 V potential window and constant current densities ranging from 0.145 to 3.47 A/g.

*Fabrication of Working Electrode:* A 10-minute ultrasonication process was used to disperse the considered sample (1.0 mg) in 250 µL of ethanol. After adding Nafion® 117 (Sigma Aldrich; 40.0µL), there was a 30-minute ultrasonication period. The dispersed solution was then drop-cast

onto the GCE (A = 0.07065 $cm^2$ ; $\phi$ = 3 mm) and allowed to dry overnight under a lamp to produce a catalyst loading of 0.976 $mg/cm^2$.

### 3.3.6 Electrochemical Sensing Measurements

The electrochemical sensing performance of the synthesized samples for $H_2O_2$ detection was assessed using a Bio-Logic EC Lab SP300 setup. A three-electrode system was used for the measurements, consisting of an Ag/AgCl reference electrode, a platinum wire for the counter electrode, and a glassy carbon electrode (GCE) for the working electrode. The electrolyte system was a 0.1 M solution of phosphate-buffered saline (PBS) containing an appropriate amount of $H_2O_2$. The prepared samples were subjected to cyclic voltammetry (CV) measurements at a scan rate of 50 mV/s to evaluate the electrochemical sensing performance. The CV scan was carried out using a 8 mM $H_2O_2$ solution, and it covered a voltage range of 1.6 V (-0.8 V to 0.8 V). The detection capability of the most favorable sample was determined by performing CV measurements with varying $H_2O_2$ concentrations ranging from 2 mM to 12 mM.

# CHAPTER 4

# Results and Discussion I

## Overview

In this chapter, characterization results for graphene oxide (GO), reduced graphene oxide (RG), and sulphur doped graphene (SG) are discussed. The techniques such as XRD, FTIR, EDS, and SEM were used for the characterization of the synthesized samples. The last section compares the electrochemical properties viz, capacitance, and $H_2O_2$ sensing properties for the samples.

## 4.1 Graphene Oxide (GO)

Fig.4.1(a) displays a low-magnification SEM image of the GO sheets with some distinctive folds and wrinkles. High-magnification image of GO as shown in Fig.4.1(b), which gives clear evidence of the peeled-off GO sheets created by the modified Hummers process and ultrasonic exfoliation process. These as-prepared GO sheets have some noticeable folds and wrinkles because of the functional groups on the surface of the oxygen-containing GO sheet [10]. The crystalline nature of a material can be revealed through X-ray diffraction (XRD) analysis. In Fig.4.2(a), the XRD pattern of GO exhibits a prominent peak at 12.22°, corresponding to the (002) plane with an inter-planar spacing of 0.721 nm. This peak confirms that the graphene sheets in GO are randomly packed. The increase in the interlayer spacing (denoted as $d$ spacing) is attributed to the intercalation of oxygen functional groups within the graphite's interlayer spacing [1]. As a result of this intercalation, the layers separate, leading to an expansion of the $d$ spacing. Furthermore, the presence of a weak diffraction peak at $2\theta$ = 42.68° is due to the graphitic crystal plane. Scherrer's equation (equation 3.2) was applied to the (002) reflection using a constant of 0.9 to determine the typical height of stacking layers. The calculated average height was found to be 4 nm for GO, which corresponds to approximately 5 graphene layers [2]. In Origin ProTM, the Pearson VII peak function was used to fit the characteristic peaks. In addition, the presence of bands in the FTIR spectra displayed in Table 4.2 provides further evidence of graphite's oxidation. When oxygen-containing groups are present, as shown in Fig. 4.2(b), the hydroxyl group's (O-H) stretching vibrations are thought to be the cause of the main absorption band in the spectrum of GO at 3171 $cm^{-1}$ [5]. The absorption peaks at 1713 $cm^{-1}$ and 1598 $cm^{-1}$ can be attributed to the C=O, C=C stretching vibrations of functional groups with carboxylic and/or carbonyl moiety and

$sp^2$ hybridized group or skeletal vibration of graphene backbone chain. According to the peak at 1226 $cm^{-1}$, the stretching vibration of the epoxy group C-O-C [39].

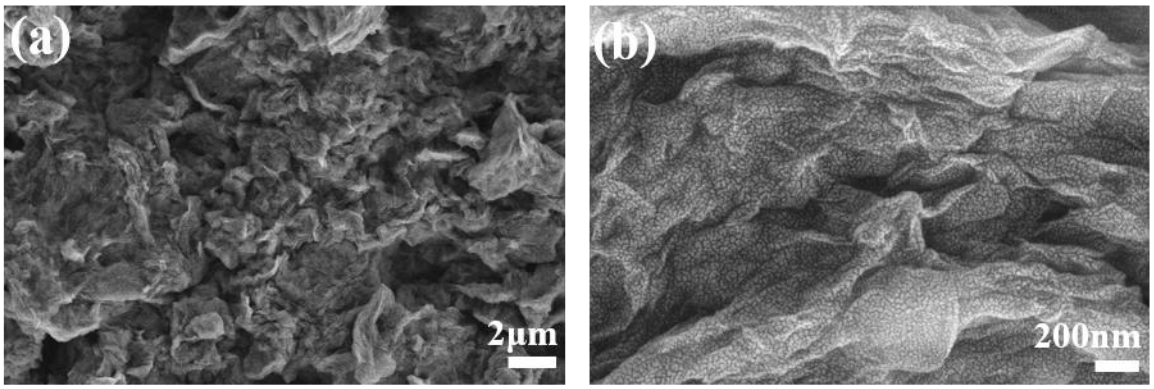


**Fig.4.1** SEM images of GO (a,b)

## 4.2 Reduced graphene oxide (RG) and sulphur doped graphene oxide (SG)

As-synthesized GO has been further used to synthesize RG and SG using the hydrothermal method. The synthesized method is discussed in section 3.2.2 and the details for the synthesized samples are also given in Table 4.1.

**Table 4.1** Details of synthesized samples.

| Sample Name | Precursor | Synthesis Method | Synthesis Temperature (°C) | Time (hrs) | Conc (mM) |
|---|---|---|---|---|---|
| RG | - | Hydrothermal method | 180 | 12 | - |
| SG | $Na_2S$ | | 180 | 12 | 2.8 |

### 4.2.1 XRD

Fig.4.2(a) displays the XRD line profiles for the synthesized samples. The sample RG exhibits a broad peak at 2θ = 24.67° (hkl 002), indicating an interlayer distance of approximately 0.34 nm. This peak confirms the successful conversion of GO into RG using the hydrothermal method. The XRD peaks of SG and RG were found to be quite similar, with no significant differences observed, except for a slight downward shift in the peak position of SG's (002) reflection compared to that of RG after the doping process. In SG, the diffractogram peak value at 2θ is measured to be 24.76° (hkl 002), corresponding to an interlayer spacing of 0.23 nm [3].

The presence of atomic sulphur species within the substance can be explained by the broad diffraction peak seen in SG. The presence of sulfur species has the capability to disrupt the interlayer structure of graphitic carbon, leading to the formation of disordered structures and the occurrence of defect sites. These defects are often associated with sulfur-containing functional groups located at the edges of graphene sheets. Furthermore, the peak observed at 78.12° corresponds to the (110) plane, indicating that the synthesized graphene does not exist exclusively as a single layer. The presence of additional peaks observed at (113), (222), (044), and (422) in the SG spectra can be ascribed to the existence of orthorhombic sulfur crystallites, as indicated by their resemblance to the corresponding peaks in the (JCPDS 00-008-0247) database [4].

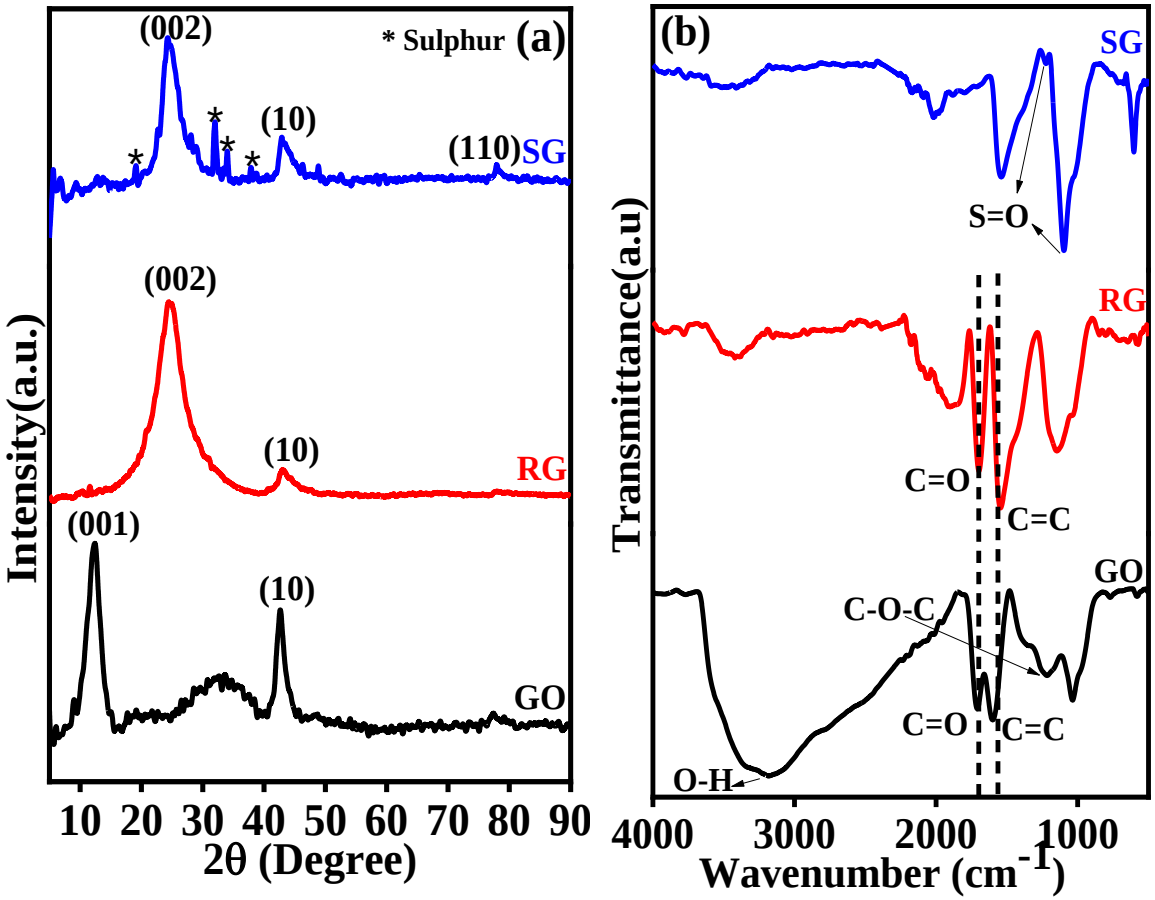


**Fig.4.2** (a) XRD of GO, RG, SG. (b) FTIR spectrum of GO, RG, SG

### 4.2.2 Fourier-transform infrared spectroscopy (FTIR)

FTIR (Fourier-transform infrared) spectroscopy is a molecular spectroscopic technique used to analyze the organic or inorganic bonds present within a system. The resulting data is typically

presented on a graph, with the x-axis representing the wavenumber ($cm^{-1}$) and the y-axis representing the percent transmittance. FTIR spectroscopy was employed to evaluate the efficiency of introducing oxygen-containing functional groups into the carbon lattice. In each spectrum, several characteristic modes associated with oxygen-containing functional groups were observed. This analysis employs infrared light energy to induce vibrations in molecular bonds, with the wavelength ranging from 4000 $cm^{-1}$ to 500 $cm^{-1}$. Fig.4.2(b) shows the FTIR spectrum for the synthesized RG and SG samples. The bands present in the FTIR spectra are used to confirm the oxidation and reduction of graphene RG, and SG samples as indicated in Table 4.2

**Table 4.2:** FTIR data analysis for the synthesized samples.

| **GO peaks ($cm^{-1}$)** | **RG peaks ($cm^{-1}$)** | **SG peaks ($cm^{-1}$)** | **Identified bonds** |
|---|---|---|---|
| 3171 | 3419 | 3437 | OH stretching vibration of the hydroxyl group |
| 1713 | 1695 | - | C=O stretching vibration of the carbonyl group |
| 1598 | 1544 | 1540 | C=C skeletal vibration of the graphene plane |
| 1226 | 1143 | - | C-O-C stretching vibration of epoxy group |
| - | - | 1097,1228 | S=O Sulphonyl group |

The spectrum of RG, and SG showed a decrease in the intensity of the O-H stretching peak at 3419 $cm^{-1}$ and 3437 $cm^{-1}$, indicating that the oxygen groups was removed during reduction. For RG, C=C is responsible for the peak at 1544 $cm^{-1}$, while C-OH is responsible for the absorption peak at 1143 $cm^{-1}$. It is worth noting that the characteristic absorption peak from the C=O bond of SG gets vanished [30]. The SG exhibits a newly noticeable distinctive peak at 1097 $cm^{-1}$ and 1228 $cm^{-1}$, which most likely corresponds to the characteristic peak of the C-S-C bond symmetrical stretching vibration but might also possibly be related to the other bonds of C-O-C and S=O [40]. These results indicated that the partial functional groups in the GO had been successfully removed by the hydrothermal and sulfonation processes.

### 4.2.3 Scanning Electron Microscopy (SEM)

Fig.4.3 shows the structural morphology of synthesized samples obtained from SEM. After hydrothermal treatment, in RG sample the graphene sheet layers are still not too well separated.

The high magification images of RG in Fig. 4.3(b) show thin, wrinkled sheets forming tulle-like structures [41]. Fig.4.3(c) shows SG sheets with more significant folds and wrinkling, very different from that of RG sheets. The surface of SG sheets exhibits more folds and distortions as a result of the functional groups' disruption of the initial conjugation and the contraction caused by the sulphur doping [8].

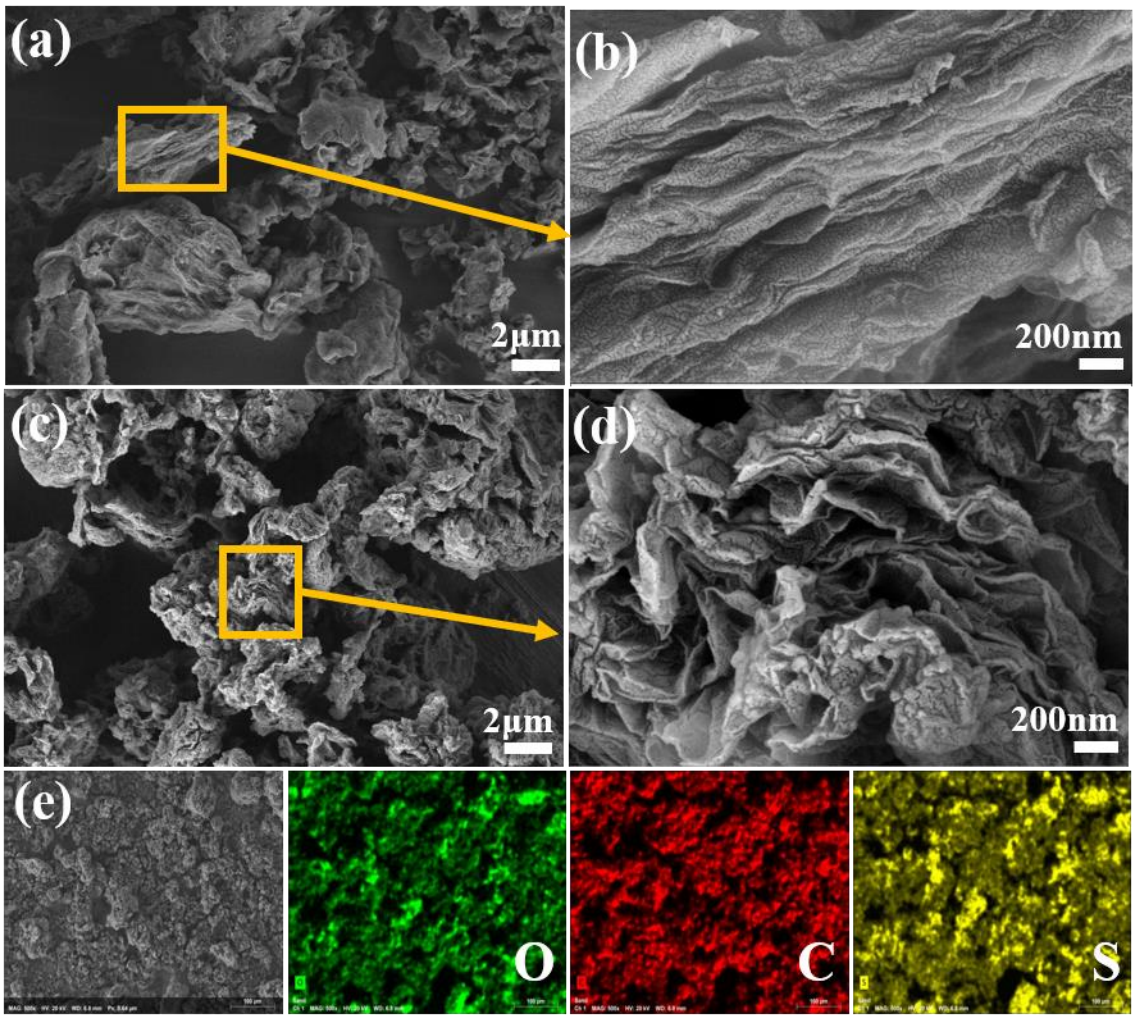


**Fig.4.3** SEM images of RG(a-b), SG(c-d) at low and high magnification and SEM-EDS mapping of SG sample (e).

The O, C, and S elements were present in the SG sample and were distributed uniformly, according to the SEM-EDS elemental mapping images displayed in Fig. 4.3(e).

### 4.2.4 Energy dispersive spectroscopy (EDS)

The EDX spectra of the RG show that the synthesized RG has distinct C and O peaks and no additional impurities, demonstrating the success of the RG synthesis shown in Fig.4.4(a).

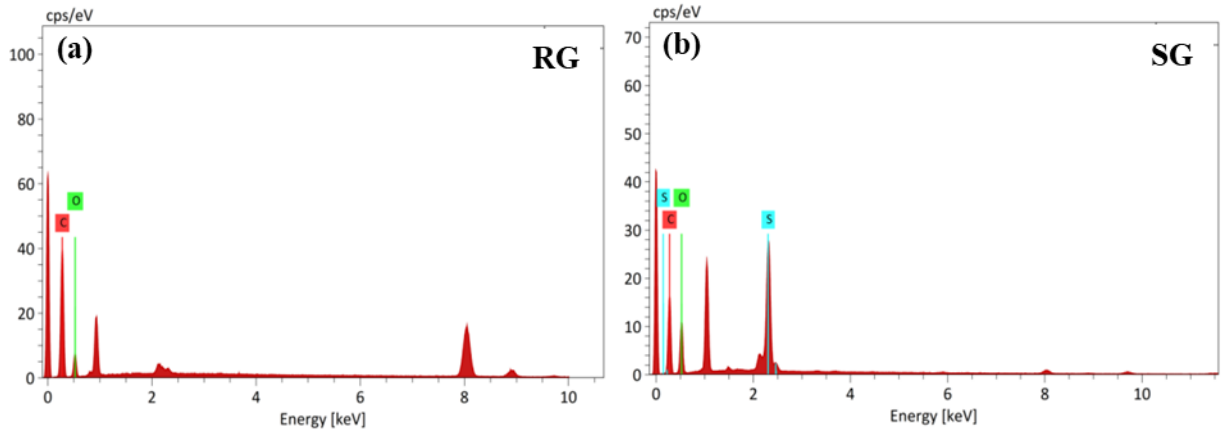


**Fig.4.4** (a) EDX of RG**,** (b) SG

Fig.4.4(b) confirms the presence of carbon, oxygen, and sulphur in SG sample from EDS. The carbon (C) atoms originate from the GO sheet framework, while the oxygen (O) atoms are derived from the functional groups of the GO sheet that contain oxygen. The sulfur (S) atoms, on the other hand, solely come from the elemental sulfur incorporated into the SG.Table 4.3 displays the percentages of carbon, oxygen, and sulphur in RG and SG respectively.

**Table 4.3** Elemental composition of SG and RG.

| **Sample** | **Carbon** | **Oxygen** | **Sulphur** |
|---|---|---|---|
| RG | 73.89% | 26.11% | - |
| SG | 65.09% | 29.79% | 5.12% |

## 4.3 Electrochemical characterizations

A comparison of electrochemical properties (super-capacitance and sensing) of synthesized samples is discussed in this chapter.

### 4.3.1 Supercapacitor measurements

In Fig.4.5 (a), the cyclic voltammetry (CV) analysis performed for all the synthesized samples using a scan rate of 10 mV $s^{-1}$ with a potential window of 1.2 V is shown. All the curves show a quasi-rectangular shape, exhibiting the characteristic behavior of electric double layer capacitance (EDLC). The area of the CV curves was maximum for the SG sample which was attributed to its maximum specific capacitance value amongest all the samples. SG sample demonstrates a significantly higher charge storage capacity compared to undoped RG and GO [30]. Fig.4.5(b) shows the galvanostatic charge/discharge curves (GCD) for the prepared samples. Each sample displayed a nearly triangular curve, which denotes electric double-layer capacitance (EDLC) dominance. The SG electrode demonstrated the longest discharge time when compared to GO and RG, which is what led to the highest capacitance value. The specific capacitance ($C_{sp}$) of the SG sample in a 1 M $H_2SO_4$ electrolyte at 3 mV/s was found to be 139.32 F $g^{-1}$, demonstrating remarkable capacitive behavior (Table 4.4). The S-doping's synergistic effect on the graphene-based electrode is primarily responsible for the SG electrode's superior electrochemical performance to the RG and GO electrodes [42].

Fig.4.5(c) demonstrates the CV measurements of SG carried out at various potential scan rates ranging from 3 mV/s to 220 mV/s. Even at a high scan rate, the CV curve's shape was without distortion. The enclosed integral area of the CV curve showed a clear increase with higher scan rates, and the current density also exhibited a gradual increase. The SG electrode material's charge-discharge analysis for different current densities ranging from 0.145 to 3.47 mA $cm^{-2}$ is shown in Fig.4.5(d). The capacitance increased at low current densities, reached a high value at lower densities, and then gradually decreased [30]. The values of specific capacitance for SG electrode were found to be 320.24 $Fg^{-1}$ and 45.61 $Fg^{-1}$, respectively, at 0.144A/g (low current density) and 3.47A/g (high current density). At higher current density values, the electrolyte ions do not have sufficient time to penetrate deeply into the interior portion of the electrode surface, so they can only access the electrode material's outer surface, and vice versa for lower current density values [42].

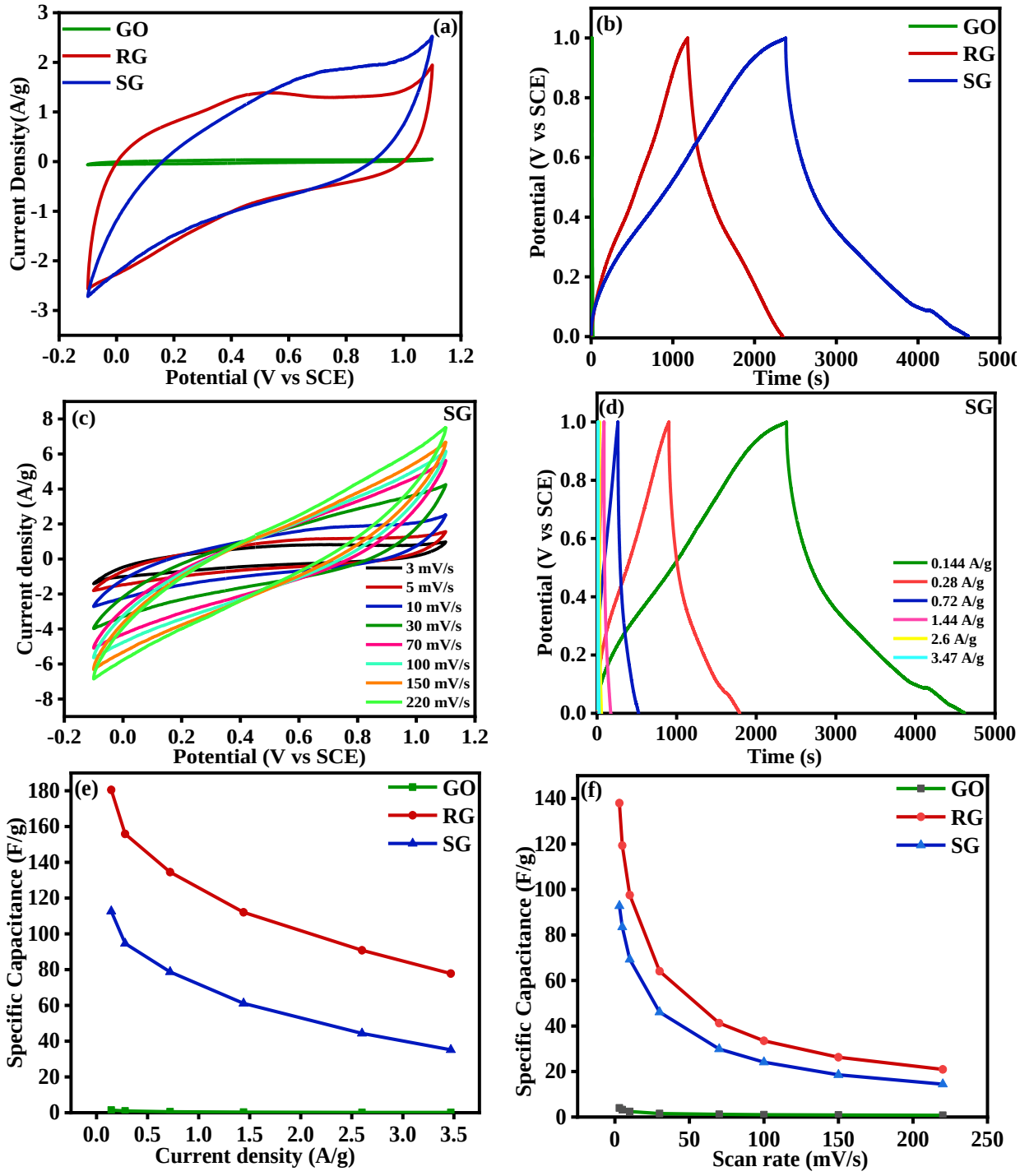


**Fig.4.5** (a) CV graphs of GO, RG, and SG at 10mVs$^{-1}$ scan rate. (b) Galvanostatic charge-discharge analysis of GO, RG, and SG at the current density of 0.145 mA cm$^{-2}$. (c) CV graph of SG at different scan rates. (d) CD analysis of SG sample at different current densities, (e)Plot of specific capacitance versus current density for GO, RG, SG. (f) Plot of specific capacitance versus scan rate for GO, RG, SG

**Table 4.4** Specific Capacitance and ECSA values of various synthesized materials.

| Sample | Specific capacitance (F/g) | | ECSA |
|---|---|---|---|
| | CV (3 mV/s) | GCD (0.145 A/g) | |
| GO | 4.00 | 1.47 | 10.64 |
| RG | 137.96 | 180.48 | 1045.5 |
| SG | 139.32 | 320.24 | 215.625 |

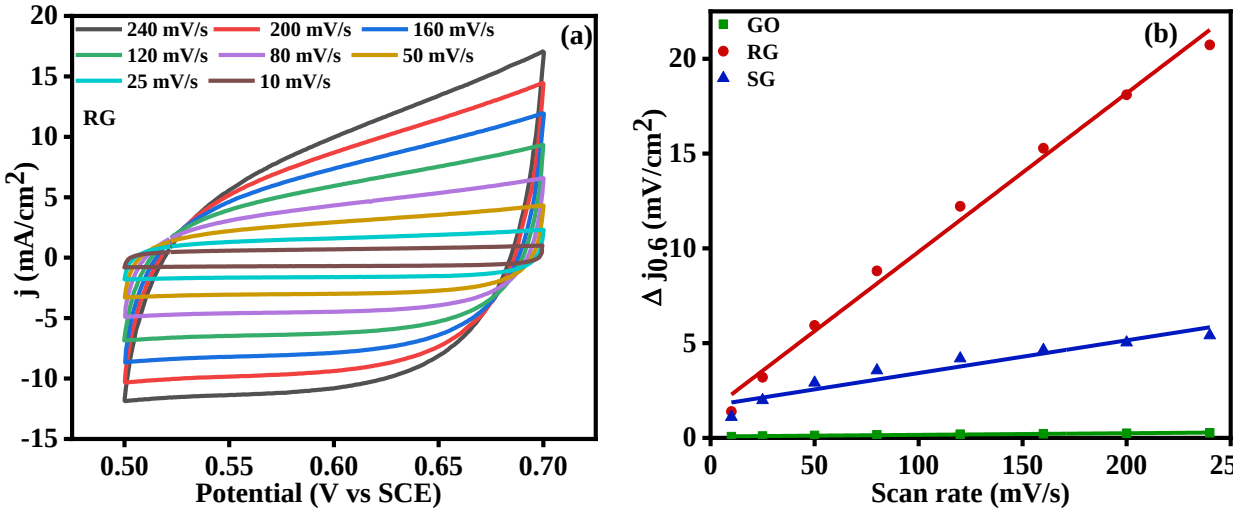


**Fig.4.6** (a) CV at different scan rates for RG, (b) Plot between scan rates and Current densities ($\Delta J_{0.6}$) of GO, RG, SG.

To further examine the electrocatalytic activities of synthesized samples, the electrochemical active surface areas (ECSA) for all the samples were determined by measuring the electrochemical double-layer capacitance ($C_{dl}$) in a non-Faradaic potential zone (0.5–0.7V). Fig.4.6(a) displays the cyclic voltammetry (CV) curve of RG at various scan rates. As the scan rate increases, the area beneath the CV curves for the RG sample increases as well, indicating an increased capacity for capacitive charge storage. Fig.4.6(b) illustrates the relationship between the current density ($\Delta J_{0.6}$) and scan rates of the samples. The analysis of these profiles by linear regression reveals that RG has a higher $C_{dl}$ value (41.82 $mFcm^{-2}$) than SG (8.62 $mFcm^{-2}$) and GO (0.42 $mFcm^{-2}$). The ECSA values were calculated using the formula ECSA= $C_{dl}/Cs$, where Cs is the specific capacitance with a standard value of 0.040 $mFcm^{-2}$ [43]. RG has a greater ECSA value of 1045.5, signifying a greater number of active sites. SG, and GO exhibit ECSA values of 215.62, and 10.64 respectively. The lower specific surface area of the SG sample may be due to the doping of the

interlayer structure due to the intercalated sulphur. These results clearly indicate that the higher capacitance of the SG sample is due to S doping and intercalated sulphur resulting in the additional pseudocapacitance contribution.

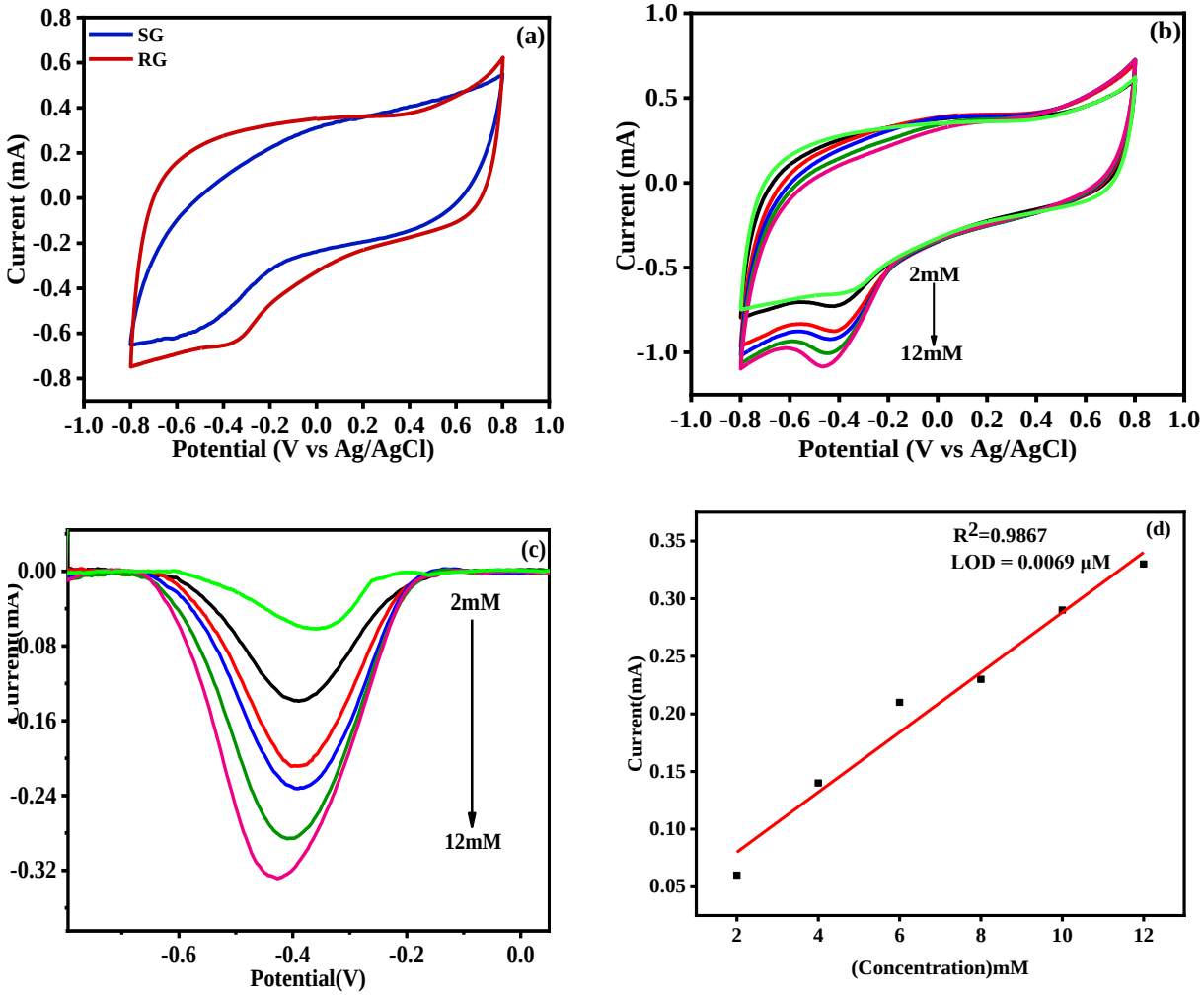


**Fig.4.7** (a) CV curves at 50mV/s scan rate for 8 mM $H_2O_2$ in 0.1 M PBS (pH-7.4) for RG, SG samples. (b) CV curves at 50mV/s scan rate for RG sample at increasing concentrations from 2mM to 12mM of $H_2O_2$ (c) Baseline-corrected reduction humps of CV curves (d) Calibration curve for RG at increasing concentrations of $H_2O_2$.

### 4.3.2 $H_2O_2$ electrochemical sensing

CV measurements were conducted on RG and SG samples to determine the optimal electrocatalyst for $H_2O_2$ reduction. Fig.4.7(a) shows the CV loops for RG and SG samples at 8 mM. The RG sample exhibited superior electrocatalytic performance compared to the SG sample, as indicated by a sharp reduction current response observed at -0.34 V. The enhanced electrocatalytic

performance of RG can be attributed to its larger electrochemically active surface area. Fig.4.7(b) illustrates the CV measurements performed on the RG sample at different $H_2O_2$ concentrations, ranging from 2 mM to 12 mM with a scan rate of 50 mV/s. The redox hump at -0.4 V was found to become more noticeable as $H_2O_2$ concentration increased serving as a fingerprint for more $H_2O_2$ desorption. The CV plot in Fig4.7(c) shows baseline-corrected reduction humps, that demonstrate a distinct increase in current with a rise in concentration. Fig.4.7(d) shows the CV curve used for calibration for the associated CV data as well as a range for linear detection that spans 2 mM to 12 mM. It was determined that the calibration curve has a correlation coefficient ($R^2$) of 0.9867. The slope of the calibration curve combined with a signal-to-noise ratio of 3 allowed for the calculation of the limit of detection (LOD), which came out to be 0.0069 μM.

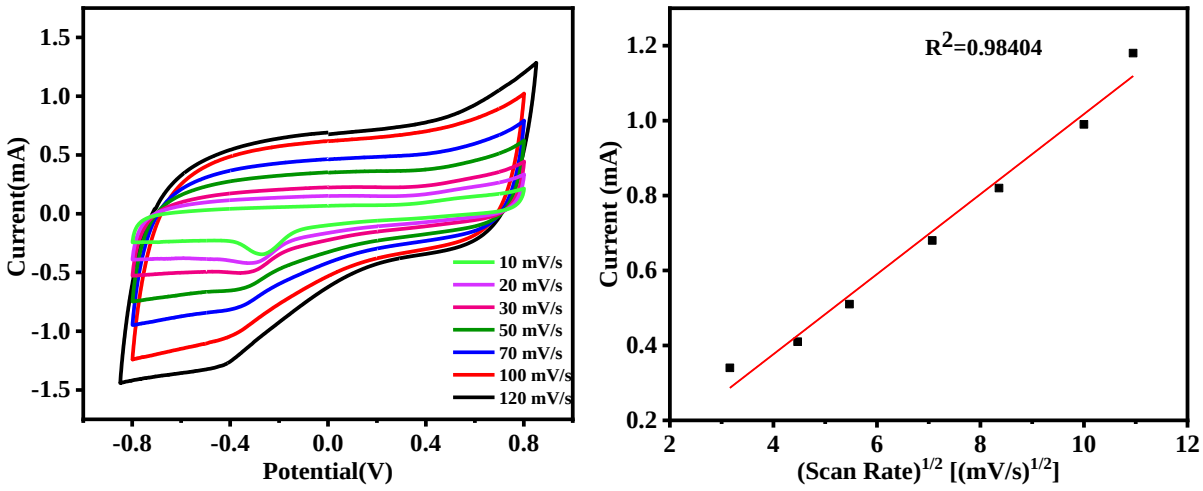


**Fig4.8** (a) CV curves of the RG electrode in a 0.1 M PBS solution (pH 7.4) containing 4 mM $H_2O_2$ at a scan rate of 10, 20, 30, 50, 70, 100, and 120 mV/s. (b) A plot of the reduction peak current against the square root of the scan rate.

In addition, we investigated the rate of potential scanning and its effect on the RG's ability to catalyze the reduction of $H_2O_2$. Cyclic voltammetry (CV) was employed to determine the effect of a changing scan rate (mV/s) on the electrochemical performance of the modified electrode. Fig.4.8(a) shows the CVs of the generated RG electrode immersed in a 0.1 M phosphate-buffered saline (PBS) solution (pH 7.4) containing 8 mM $H_2O_2$. The measurements were conducted at scan rates ranging from 10 to 120 mV/s.

The observed reduction current peak is indicative of the reduction process of $H_2O_2$. We noticed that the reduction peak current response for the reduction of $H_2O_2$ increased with an increasing

scan rate of 10-120 mV/s. The reduction peak current responses were calibrated against the square root of the scan rate, and the resulting calibration curve is shown in Fig.4.8(b). This calibration curve demonstrates a linear relationship, indicating that the reduction in peak current response increases proportionally. This implies that the electron transfer process of RG follows a diffusion-controlled electrochemical process [42]. This indicates that the redox processes of $H_2O_2$ on the RG electrode were controlled by diffusion suggesting that the diffusion-controlled mechanism plays a crucial role in the performance of these electrodes [44]. It provides an effective and efficient approach for the detection of hydrogen peroxide, enabling selective, sensitive, rapid, and reliable analysis in a variety of applications, including biosensors, environmental monitoring, and clinical diagnostics.

# CHAPTER 5

# Results and Discussion II

This chapter discusses the characterization results for the synthesized curcumin@graphene based composites have been discussed.

## 5.1 Curcumin

Fig. 5.1(a) shows the curcumin X-ray diffraction pattern. The diffractogram pattern of curcumin shows characteristic peaks at a 2θ (14.36, 17.20, 18.02, 24.78, 25.86, and 27.36). These peaks imply that curcumin has a highly crystalline structure in powder form.

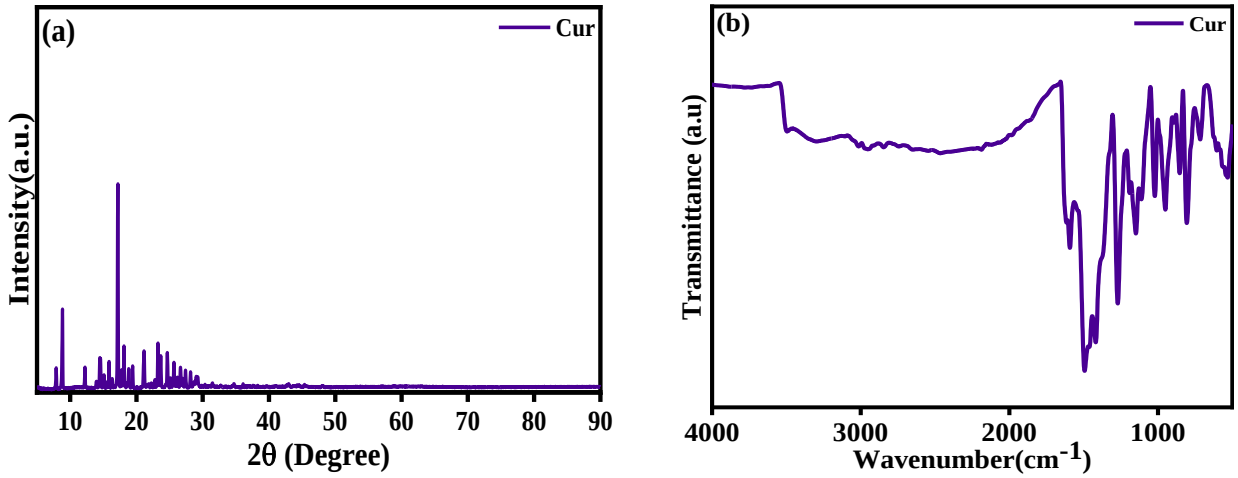


**Fig.5.1** (a) XRD analysis of curcumin, (b) FTIR analysis of curcumin

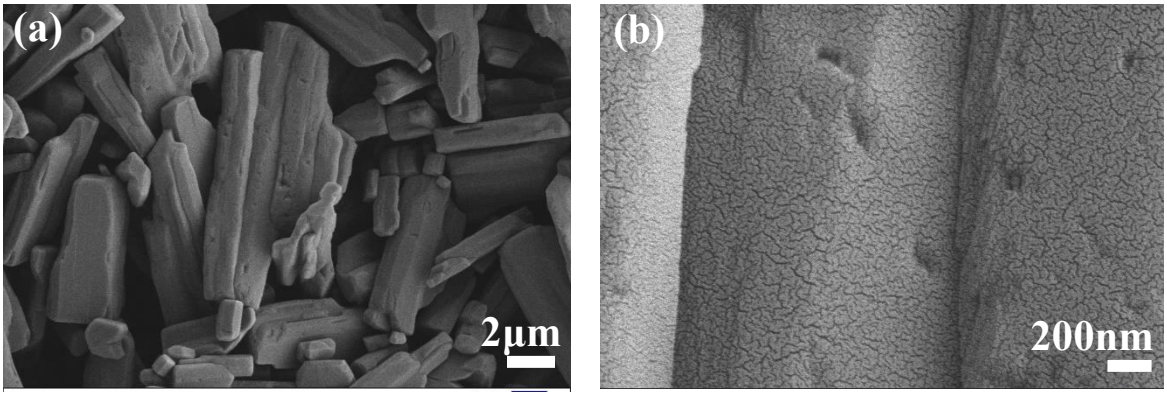


**Fig.5.2** SEM micrographs of curcumin

Fig.5.1(b) shows the FTIR spectra of curcumin. Characteristics peaks of curcumin are observed at 3498, 1583, 1268, 1147, and 950 $cm^{-1}$, which were caused by the stretching vibrations of O-H, C=O, C-O, C-O-C, C-O, and C-H, respectively [45]. Fig.5.2 shows the SEM image of curcumin at low and high magnification. The pure curcumin showed an irregular, flat, and rod-like structure with particle size ranging in length from 1.3 to 42 μm as shown in image Fig.5.2(a). Under high magnification, the surface of curcumin exhibits irregularities and cracks.

## 5.2 Curcumin@graphene composites

In this section, curcumin has been used to synthesize the graphene-based composites (Curcumin@graphene) using oil bath heat treatment. The details of as obtained composites are given in Table 5.1 and the method is discussed in section 3.2.3.

**Table 5.1** Details of synthesized Curcumin@graphene composites

| Sample Name | Synthesis method | Precursor | Precursor: Curcumin (w/w) |
|---|---|---|---|
| GO-Cur | Oil bath heat treatment | GO | 1**:**0.5 |
| SG-Cur | | SG | 1**:**0.5 |
| RG-Cur | | RG | 1.43**:** 0.71 |

### 5.2.1 XRD

Fig.5.3 shows the XRD pattern for the synthesized curcumin@graphene composites. For the GO-Cur composite the (002) peak at 2θ = 12.22°, vanished, and a new peak with a signature of reduced GO at 2θ = 25.38° and a d-spacing of 0.35 nm appeared as shown in Fig.5.3(a) [34]. This indicated that GO was reduced in the presence of curcumin. Similarly, the intense peaks observed at 2θ = 24.85°, 25.07° of SG-Cur, and RG-Cur respectively. Additionally, the presence of a weak diffraction peak at $2\theta$ = 43.01° suggests that the reduction process was incomplete. During the washing of curcumin@graphene composites, the resulting supernatant exhibited a yellow color, indicating incomplete incorporation of curcumin into the composites. The absence of curcumin crystalline peaks in the X-ray diffraction result suggests that the amount of curcumin integrated into the composites is lower than that of graphene [1].

### 5.2.2 FTIR

Fig.5.3(b) shows the spectra of curcumin composites. The FTIR spectra of the GO-Cur composite demonstrates distinctive curcumin absorption features at 1574, 1272, and 1153 $cm^{-1}$, which are similar to those of curcumin alone. For the synthesized composites, the C-O-C band peak at 1037 $cm^{-1}$ and the carboxylic group vibrational absorption band peak at 1714 $cm^{-1}$ both diminished significantly. The characteristic peaks around 1509, 1217, and 1147 $cm^{-1}$ were also present in the other composites, i.e. SG-Cur and RG-Cur indicating that they also contained curcumin as shown in Fig.5.3(b). The intensity of the O-H vibration band of all the composites reduced showing that curcumin had been effectively grafted onto SG-Cur and RG-Cur composites. The results demonstrate substantial incorporation of curcumin within the curcumin@graphene composites

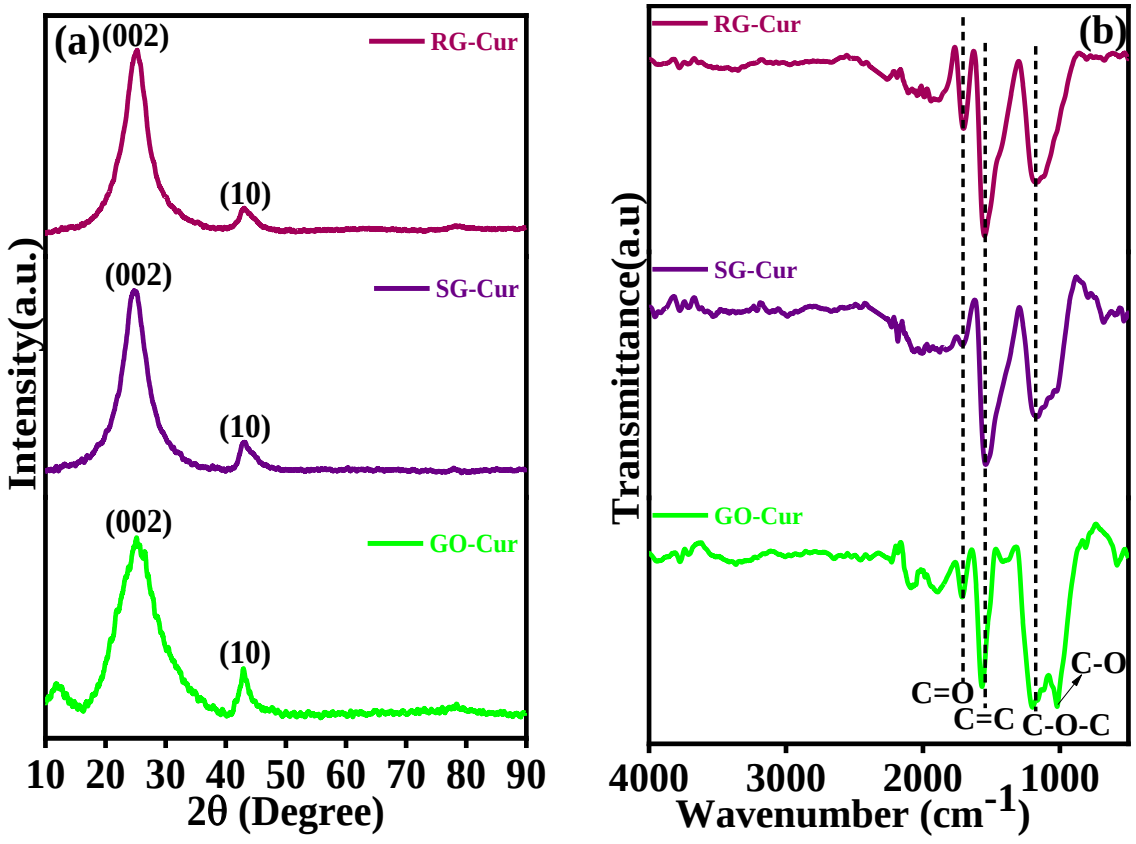


**Fig.5.3** (a) XRD analysis of GO-Cur, SG-Cur, RG-Cur (b) FTIR analysis of GO-Cur, SG-Cur, RG-Cur

### 5.2.3 SEM

For the SEM analysis of GO-Cur, SG-Cur, and RG-Cur, the samples were dispersed in ethanol using utrasonification. The SEM micrographs (Fig.5.4) show that the GO-Cur, SG-Cur, and RG-Cur were completely exfoliated. The physical attachment of graphene flakes to the surface of curcumin complexes in SEM images confirms the conjugation of curcumin with graphene in the synthesized samples [34]. Curcumin particles adhere to GO, RG, and SG, as shown in Fig.5.4 Because the oxygen functional groups were removed and curcumin was attached, the sheet-like morphology of the graphene flakes is preserved with a slight agglomeration or shortening of the flakes within the curcumin@graphene composites.

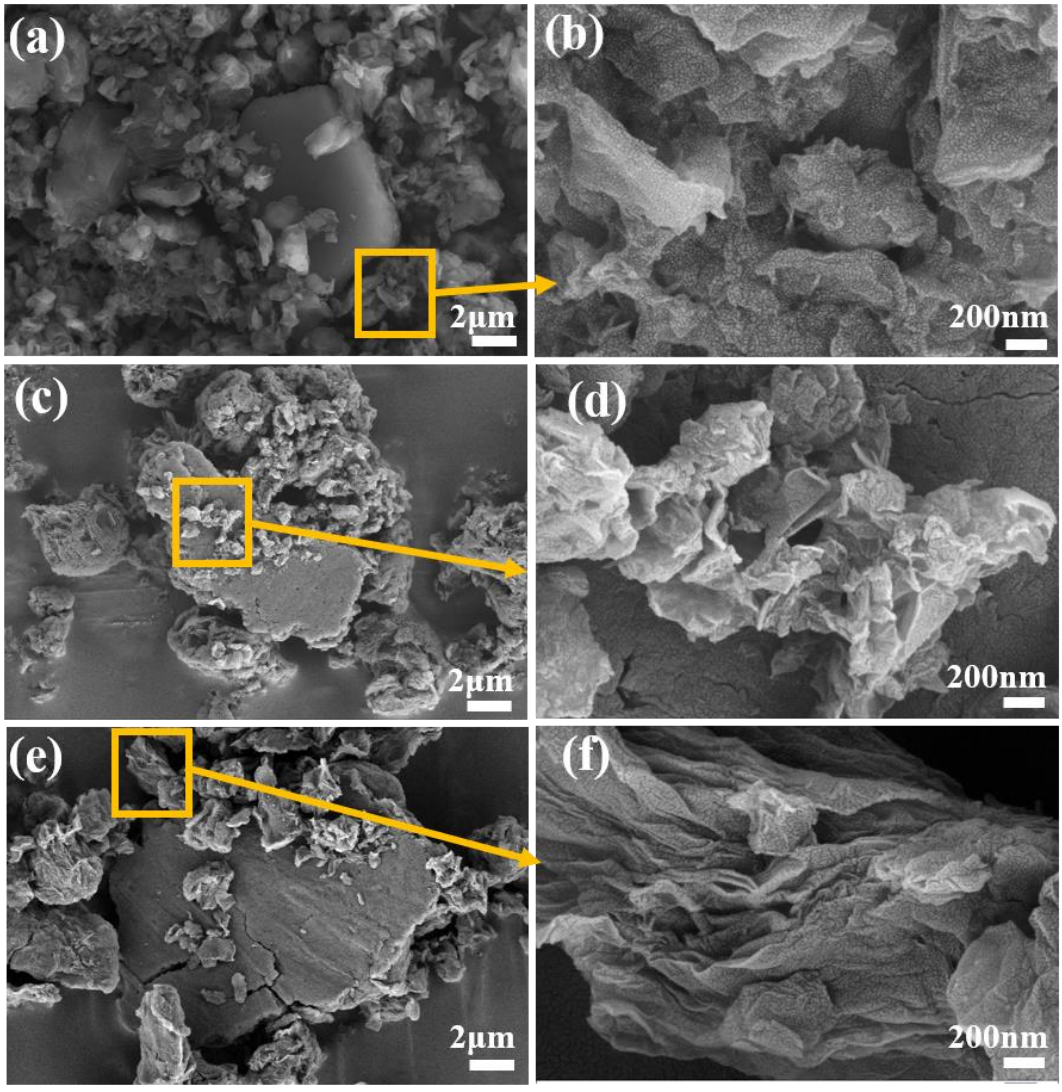


**Fig.5.4** SEM micrographs of GO-Cur(a-b), SG-Cur(c-d), RG-Cur(e-f)

## 5.3 Electrochemical measurements

This section shows the comparison of super capacitance and electrochemical sensing of the synthesized curcumin-based composites.

### 5.3.1 Supercapacitor measurements

In Fig. 5.5(a), The obtained cyclic voltammetry (CV) data, recorded at a scan rate of 10 mV/s, reveal that all the loops have a distorted rectangular shape. This characteristic suggests that the samples possess excellent capacitance properties. Among the curcumin@graphene composites, SG-Cur composite has the largest CV curve area and the strongest redox peak intensity, both of which are indicative of greatly increased specific capacitance and rapid redox process kinetics. The strong interlinking between sulphur and curcumin in the SG-Cur composite enables efficient charge migration, leading to a higher percentage of pseudocapacitance. This interlinking enhances the capacitive behaviour of the material as a whole by facilitating electrochemical reactions at the interface between the electrode and the electrolyte. The charge-discharge curves in Fig.5.5(b) demonstrate nearly triangular shapes for all samples, indicating that they predominantly exhibit electric double-layer capacitance (EDLC) behavior. The SG-Cur composite shows the widest charge-discharge curve among the composites, leading to the highest capacitance value. Figure 5.5(c) shows the CV measurements of the SG-Cur composite at various potential scan rates. Even at high scan rates, the CV curve maintains its shape without distortion. The enclosed integral area of the CV curve and the current density both increase with higher scan rates, indicating enhanced capacitive behavior. The specific capacitance (Csp) of the SG-Cur composite in a 1 M $H_2SO_4$ electrolyte at 3 mV/s was found to be 214.18 F $g^{-1}$ (Table 5.2). By analyzing the GCD curves at various current densities as shown in Fig.5.5(d), it is observed that the capacitance initially rises at lower current densities, reaches a maximum value, and then gradually declines. This behaviour may be related to the fact that the electrolyte ions only partially penetrate the electrode material at higher current densities, mainly accessing the outer surface.

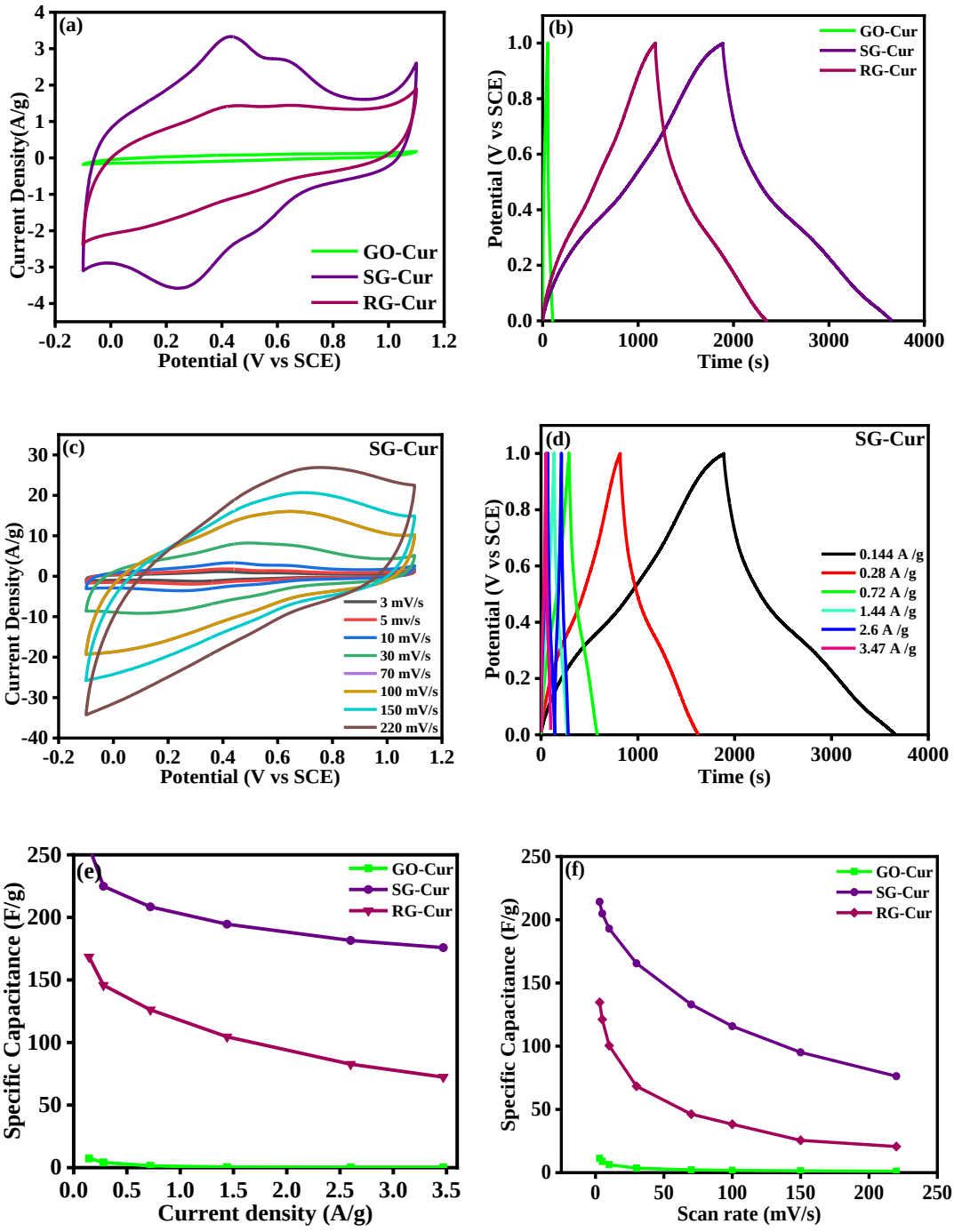


**Fig.5.5** (a) (a) CV graphs of GO-Cur, SG-Cur, RG-Cur at 10 mV $s^{-1}$ scan rate, (b) Galvanostatic charge-discharge analysis of GO-Cur, SG-Cur, RG-Cur at the current density of 0.144 mA $cm^{-2}$, (c) CV graph of SG-Cur at different scan rates, (d) CD analysis of SG-Cur sample at different current densities, (e) specific capacitance variation as a function of the current density of GO-Cur, SG-Cur, RG-Cur, (f) specific capacitance variation as a function of scan rate of GO-Cur, SG-Cur, RG-Cur.

Fig.5.5(e) shows the specific capacitance plot for the synthesized samples as a function of scan rate. The measured specific capacitance values from the galvanostatic charge-discharge (GCD) graphs at various current densities and scan rates are shown in Fig.5.5(f). The highly porous structure, chemical stability, and high surface area of the curcumin@graphene composite electrode are believed to be the reasons behind its excellent electrochemical performance [12][46].

**Table 5.2** Specific capacitance and ECSA values of the synthesized materials.

| Specific capacitance (F/g) | GO | GO-Cur | SG | SG-Cur | RG | RG-Cur |
|---|---|---|---|---|---|---|
| **CV (3mV/s)** | 4.00 | 11.40 | 139.32 | 214.18 | 137.96 | 134.71 |
| **GCD (0.145A/g)** | 1.47 | 7.40 | 320.24 | 256.48 | 180.48 | 168.42 |
| **ECSA** | 10.645 | 33.25 | 215.625 | 2021 | 1045.5 | 143.87 |

Furthermore, the electrochemical surface area (ECSA) of synthesized composites was measured using cyclic voltammetry (CV) within a non-Faradaic potential zone (0.5–0.7 V) in 1M $H_2SO_4$ as the supporting electrolyte at varying scan rates. Fig.5.6(a) shows the CV curves of the SG-Cur composite at different scan rates. Fig.5.6(b) illustrates the relationship between scan rates and the current density ($\Delta J_{0.6}$) of the synthesized composites. Linear regression analysis of these curves reveals that SG-Cur exhibits a higher $C_{dl}$ value (80.84 $mFcm^{-2}$) compared to RG-Cur (5.75 $mFcm^{-2}$). The ECSA value of all the synthesized composites is shown in Table 5.2.

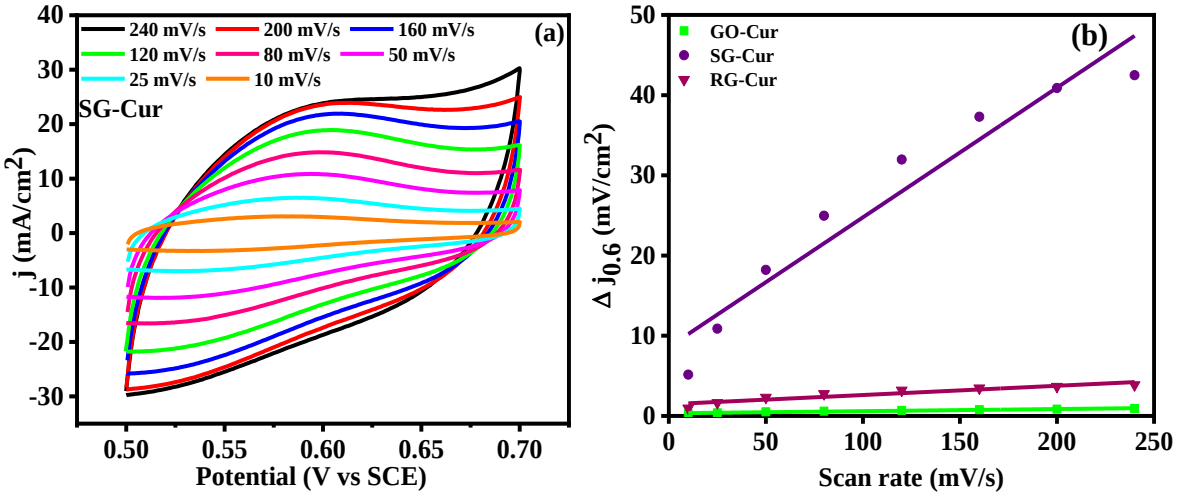


**Fig.5.6** (a) CV at different scan rates for SG-Cur, (b) Plot between current densities ($\Delta J_{0.6}$) and scan rates of GO-Cur, SG-Cur, RG-Cur.

Further reduction of the RG-Cur composite during the synthesis process may cause an increase in agglomeration and shortening of flakes. As a result, the interaction between the reduced graphene and curcumin might become weaker. Moreover, the significant decrease in the surface area of RG-Cur is indicative of the structural changes caused by the reduction process. On the other hand, the notable increase in the surface area observed in SG-Cur suggests a reduction in the incorporation of sulphur within curcumin, resulting in the development of a structure with more porosity. The higher ECSA of SG-Cur suggests that it has a greater number of active sites, which may be a key factor in its enhanced catalytic activity [47].

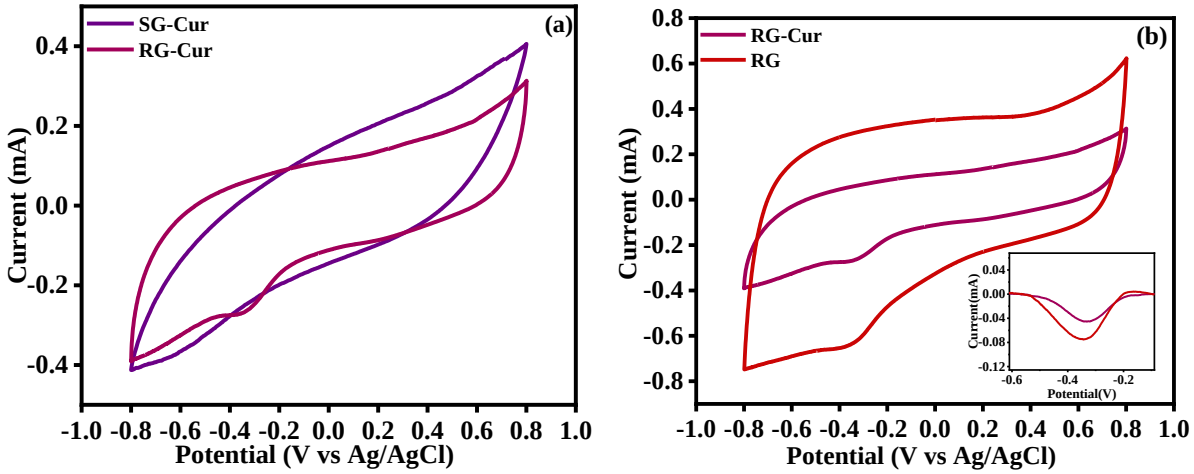


**Fig.5.7** (a) CV curves at 50mV/s scan rate for 8 mM $H_2O_2$ in 0.1 M PBS (pH-7.4) SG- Cur, RG-Cur composites. (b) baseline-corrected cathodic humps of the CV loop for RG, RG-Cur at 8 mM.

## 5.3.2 $H_2O_2$ electrochemical sensing

Curcumin@graphene composites were tested using cyclic voltammetry for $H_2O_2$ detection. Fig.5.7(a) displays the CV loop for the SG-Cur and RG-Cur samples at 8 mM $H_2O_2$ in 0.1 M PBS (pH-7.4). The superior electrocatalytic sensing performance of RG-Cur is evident from the presence of a distinct cathodic peak at -0.3 V. On the other hand, the absence of a cathodic peak in the CV curve of the SG-Cur electrode as shown in Fig.5.7 (a) indicates limitations in its potential as an electrochemical sensor for $H_2O_2$ detection. In Figure 5.7(b) and the inset of Fig.5.7(c), the baseline-corrected cathodic humps of the CV loop for RG and RG-Cur at 8 mM are depicted. It can be observed that RG exhibits an intense cathodic peak due to its high surface area. However, after the interlinking with curcumin, the surface area of RG reduces, resulting in lower electrochemical sensing properties.

# CHAPTER 6

# Conclusions

Reduced graphene oxide (RG), sulphur-doped graphene (SG), and their respective composites with curcumin were synthesized and characterized for super capacitance and $H_2O_2$ electrochemical sensing applications. RG and SG were prepared by a green one-pot hydrothermal method at a low temperature of 180º C. These samples were further used in oil bath heat treatment to synthesize the Curcumin@Graphene composites. The successful incorporation of sulphur and reduction of graphene oxide in the samples was confirmed through XRD analysis, while SEM imaging provided visual information on morphological features and structural alterations. Additionally, FTIR spectra offered valuable insights into the chemical functional groups and bonding characteristics of the materials. The SG electrode displayed a remarkable specific capacitance (Csp) of 139.32 F/g in 1M $H_2SO_4$ at a scan rate of 3 mV/s which further enhanced by the incorporation of curcumin (SG-Cur). The SG-Cur composite showed excellent capacitance of 214.18 F/g at 3 mV/s and also had a higher ECSA value = 2021, indicating that the presence of curcumin increases its surface area. The RG sample exhibited exceptional performance in detecting hydrogen peroxide, with a remarkable limit of detection (LOD) of 0.0069 μM within the concentration range of 2-12 mM. The highly porous structure, chemical stability, and high specific surface area of the curcumin@graphene composite electrode are believed to be the reasons behind their excellent supercapacitance. Reduced sensing performance of Curcumin@graphene samples for $H_2O_2$ detection can be attributed to interlinking between curcumin and graphene-based samples resulting in decrease ECSA.

# CHAPTER 7

# References


1. Hidayah, N.M.S.; Liu, W.W.; Lai, C.W.; Noriman, N.Z.; Khe, C.S.; Hashim, U.; Lee, H.C. Comparison on Graphite, Graphene Oxide and Reduced Graphene Oxide: Synthesis and Characterization. *AIP Conf. Proc.* **2017**, *1892*, doi:10.1063/1.5005764.

2. Le Ba, T.; Mahian, O.; Wongwises, S.; Szilágyi, I.M. Review on the Recent Progress in the Preparation and Stability of Graphene-Based Nanofluids. *J. Therm. Anal. Calorim.* **2020**, *142*, 1145–1172, doi:10.1007/s10973-020-09365-9.

3. Mirmohseni, A.; Azizi, M.; Seyed Dorraji, M.S. Facile Synthesis of Copper/ Reduced Single Layer Graphene Oxide as a Multifunctional Nanohybrid for Simultaneous Enhancement of Antibacterial and Antistatic Properties of Waterborne Polyurethane Coating. *Prog. Org. Coatings* **2019**, *131*, 322–332, doi:10.1016/j.porgcoat.2019.02.031.

4. Smith, A.T.; LaChance, A.M.; Zeng, S.; Liu, B.; Sun, L. Synthesis, Properties, and Applications of Graphene Oxide/Reduced Graphene Oxide and Their Nanocomposites. *Nano Mater. Sci.* **2019**, *1*, 31–47, doi:10.1016/j.nanoms.2019.02.004.

5. Yu, W.; Sisi, L.; Haiyan, Y.; Jie, L. Progress in the Functional Modification of Graphene/Graphene Oxide: A Review. *RSC Adv.* **2020**, *10*, 15328–15345, doi:10.1039/d0ra01068e.

6. Lee, S.J.; Theerthagiri, J.; Nithyadharseni, P.; Arunachalam, P.; Balaji, D.; Madan Kumar, A.; Madhavan, J.; Mittal, V.; Choi, M.Y. Heteroatom-Doped Graphene-Based Materials for Sustainable Energy Applications: A Review. *Renew. Sustain. Energy Rev.* **2021**, *143*, 110849, doi:10.1016/j.rser.2021.110849.

7. Kumar, R.; Sahoo, S.; Joanni, E.; Singh, R.K.; Maegawa, K.; Tan, W.K.; Kawamura, G.; Kar, K.K.; Matsuda, A. Heteroatom Doped Graphene Engineering for Energy Storage and Conversion. *Mater. Today* **2020**, *39*, 47–65, doi:10.1016/j.mattod.2020.04.010.

8. Duraivel, M.; Nagappan, S.; Balamuralitharan, B.; Selvam, S.; Karthick, S.N.; Prabakar, K.; Ha, C.S.; Kim, H.J. Superior One-Pot Synthesis of a Doped Graphene Oxide Electrode for a High Power Density Supercapacitor. *New J. Chem.* **2018**, *42*, 11093–11101, doi:10.1039/c8nj01672k.

9. Chen, Y.; Li, J.; Mei, T.; Hu, X.; Liu, D.; Wang, J.; Hao, M.; Li, J.; Wang, J.; Wang, X. Low-Temperature and One-Pot Synthesis of Sulfurized Graphene Nanosheets via in Situ Doping and Their Superior Electrocatalytic Activity for Oxygen Reduction Reaction. *J. Mater. Chem. A* **2014**, *2*, 20714–20722, doi:10.1039/c4ta04938a.

10. Zhengshan Tian, ab Jitao Li, b Gangyi Zhu, b Junfeng Lu, b Yueyue Wang, b Z.S.C.X. Facile Synthesis of Highly Conductive Sulfur-Doped Reduced Graphene Oxide Sheets. *J. Mater. Chem. C* **2015**, *3*, 10715–10722, doi:10.1039/b000000x.

11. Maleki Dizaj, S.; Sharifi, S.; Tavakoli, F.; Hussain, Y.; Forouhandeh, H.; Hosseiniyan Khatibi, S.M.; Memar, M.Y.; Yekani, M.; Khan, H.; Goh, K.W.; et al. Curcumin-Loaded Silica Nanoparticles: Applications in Infectious Disease and Food Industry. *Nanomaterials* **2022**, *12*, 1–16, doi:10.3390/nano12162848.

12. Jyothibasu, J.P.; Lee, R.H. Green Synthesis of Polypyrrole Tubes Using Curcumin Template for Excellent Electrochemical Performance in Supercapacitors. *J. Mater. Chem. A* **2020**, *8*, 3186–3202, doi:10.1039/c9ta11934e.

13. Hatamie, S.; Ahadian, M.M.; Iraji zad, A.; Akhavan, O.; Jokar, E. Photoluminescence and Electrochemical Investigation of Curcumin-Reduced Graphene Oxide Sheets. *J. Iran. Chem. Soc.* **2018**, *15*, 351–357, doi:10.1007/s13738-017-1236-4.

14. Kharangarh, P.R.; Singh, G. Facile Synthesis of Sulfur Doped Graphene Quantum Dots for High Performance Supercapacitor Applications. *Integr. Ferroelectr.* **2019**, *202*, 163–170, doi:10.1080/10584587.2019.1674834.

15. Zhang, Q.; Wang, L.; Li, G.; Liu, Y. A Real-Time Energy Management Control Strategy for Battery and Supercapacitor Hybrid Energy Storage Systems of Pure Electric Vehicles. *J. Energy Storage* **2020**, *31*, 101721, doi:10.1016/j.est.2020.101721.

16. Shao, Y.; Wang, J.; Wu, H.; Liu, J.; Aksay, I.A.; Lin, Y. Graphene Based Electrochemical Sensors and Biosensors: A Review. *Electroanalysis* **2010**, *22*, 1027–1036, doi:10.1002/elan.200900571.

17. Kanuganti, S.R.; Sultana, R.; Kolli, D.; Maddula, G.K.; Singampalli, M.R. Facile One Pot Synthesis of Sulphur Doped Graphene for Non-Enzymatic Sensing of Hydrogen Peroxide. *Int. J. Environ. Anal. Chem.* **2021**, *00*, 1–12, doi:10.1080/03067319.2021.1980785.

18. Chen, J.; Yao, B.; Li, C.; Shi, G. An Improved Hummers Method for Eco-Friendly Synthesis of Graphene Oxide. *Carbon N. Y.* **2013**, *64*, 225–229, doi:10.1016/j.carbon.2013.07.055.

19. Chong, S.W.; Lai, C.W.; Abdul Hamid, S.B. Green Preparation of Reduced Graphene Oxide Using a Natural Reducing Agent. *Ceram. Int.* **2015**, *41*, 9505–9513, doi:10.1016/j.ceramint.2015.04.008.

20. Zaaba, N.I.; Foo, K.L.; Hashim, U.; Tan, S.J.; Liu, W.W.; Voon, C.H. Synthesis of Graphene Oxide Using Modified Hummers Method: Solvent Influence. *Procedia Eng.* **2017**, *184*, 469–477, doi:10.1016/j.proeng.2017.04.118.

21. Zhang, Q.; Yang, Y.; Fan, H.; Feng, L.; Wen, G.; Qin, L.C. Synthesis of Graphene Oxide Using Boric Acid in Hummers Method. *Colloids Surfaces A Physicochem. Eng. Asp.* **2022**, *652*, 129802, doi:10.1016/j.colsurfa.2022.129802.

22. Chen, X.; Qu, Z.; Liu, Z.; Ren, G. Mechanism of Oxidization of Graphite to Graphene Oxide by the Hummers Method. *ACS Omega* **2022**, *7*, 23503–23510, doi:10.1021/acsomega.2c01963.

23. Méndez-Lozano, N.; Pérez-Reynoso, F.; González-Gutiérrez, C. Eco-Friendly Approach

for Graphene Oxide Synthesis by Modified Hummers Method. *Materials (Basel).* **2022**, *15*, doi:10.3390/ma15207228.

24. Cao, N.; Zhang, Y. Study of Reduced Graphene Oxide Preparation by Hummers' Method and Related Characterization. *J. Nanomater.* **2015**, *2015*, doi:10.1155/2015/168125.

25. Zhang, Z.; Shi, X.; Yang, X.; Fu, Y.; Zhang, K.; Lai, Y.; Li, J. Nanooctahedra Particles Assembled FeSe2 Microspheres Embedded into Sulfur-Doped Reduced Graphene Oxide Sheets As a Promising Anode for Sodium Ion Batteries. *ACS Appl. Mater. Interfaces* **2016**, *8*, 13849–13856, doi:10.1021/acsami.5b12148.

26. Raghavan, N.; Thangavel, S.; Sivalingam, Y.; Venugopal, G. Investigation of Photocatalytic Performances of Sulfur Based Reduced Graphene Oxide-TiO 2 Nanohybrids. *Appl. Surf. Sci.* **2018**, *449*, 712–718, doi:10.1016/j.apsusc.2018.01.043.

27. Siddiqui, A.S.; Hayat, A.; Nawaz, M.H.; Ahmad, M.A.; Nasir, M. Effect of Sulfur Doping on Graphene Oxide towards Amplified Fluorescence Quenching Based Ultrasensitive Detection of Hydrogen Peroxide. *Appl. Surf. Sci.* **2020**, *509*, 144695, doi:10.1016/j.apsusc.2019.144695.

28. Tarimo, D.J.; Oyedotun, K.O.; Mirghni, A.A.; Sylla, N.F.; Manyala, N. High Energy and Excellent Stability Asymmetric Supercapacitor Derived from Sulphur-Reduced Graphene Oxide/Manganese Dioxide Composite and Activated Carbon from Peanut Shell. *Electrochim. Acta* **2020**, *353*, 136498, doi:10.1016/j.electacta.2020.136498.

29. Zhang, M.; Song, Z.; Liu, H.; Wang, A.; Shao, S. MoO2 Coated Few Layers of MoS2 and FeS2 Nanoflower Decorated S-Doped Graphene Interoverlapped Network for High-Energy Asymmetric Supercapacitor. *J. Colloid Interface Sci.* **2021**, *584*, 418–428, doi:10.1016/j.jcis.2020.10.005.

30. Rosli, N.H.A.; Lau, K.S.; Winie, T.; Chin, S.X.; Chia, C.H. Synergistic Effect of Sulfur-Doped Reduced Graphene Oxide Created via Microwave-Assisted Synthesis for Supercapacitor Applications. *Diam. Relat. Mater.* **2021**, *120*, 108696, doi:10.1016/j.diamond.2021.108696.

31. Hatamie, S.; Akhavan, O.; Sadrnezhaad, S.K.; Ahadian, M.M.; Shirolkar, M.M.; Wang, H.Q. *Curcumin-Reduced Graphene Oxide Sheets and Their Effects on Human Breast Cancer Cells*; Elsevier B.V., 2015; Vol. 55; ISBN 9821661645.

32. Elavarasi, G.; Sivasakthi, J.; Amutha, M.; Jeyaprabha, B.; Prakash, P.; Gubendran, A. Synthesis, Characterization and Antimicrobial Activity of Multifunctional Graphene Oxide-Curcumin Scaffold. *Iosr-Jpbs* **2016**, *11*, 33–38, doi:10.9790/3008-1105043338.

33. Bugli, F.; Cacaci, M.; Palmieri, V.; Di Santo, R.; Torelli, R.; Ciasca, G.; Di Vito, M.; Vitali, A.; Conti, C.; Sanguinetti, M.; et al. Curcumin-Loaded Graphene Oxide Flakes as an Effective Antibacterial System against Methicillin-Resistant Staphylococcus Aureus. *Interface Focus* **2018**, *8*, 1–8, doi:10.1098/rsfs.2017.0059.

34. De, D.; Das, C.K.; Mandal, D.; Mandal, M.; Pawar, N.; Chandra, A.; Gupta, A.N. Curcumin

Complexed with Graphene Derivative for Breast Cancer Therapy. *ACS Appl. Bio Mater.* **2020**, *3*, 6284–6296, doi:10.1021/acsabm.0c00771.

35. Nowroozi, N.; Faraji, S.; Nouralishahi, A.; Shahrousvand, M. Biological and Structural Properties of Graphene Oxide/Curcumin Nanocomposite Incorporated Chitosan as a Scaffold for Wound Healing Application. *Life Sci.* **2021**, *264*, 118640, doi:10.1016/j.lfs.2020.118640.

36. Khan, H.; Yerramilli, A.S.; D'Oliveira, A.; Alford, T.L.; Boffito, D.C.; Patience, G.S. Experimental Methods in Chemical Engineering: X-Ray Diffraction Spectroscopy—XRD. *Can. J. Chem. Eng.* **2020**, *98*, 1255–1266, doi:10.1002/cjce.23747.

37. Surekha, G.; Krishnaiah, K.V.; Ravi, N.; Padma Suvarna, R. FTIR, Raman and XRD Analysis of Graphene Oxide Films Prepared by Modified Hummers Method. *J. Phys. Conf. Ser.* **2020**, *1495*, doi:10.1088/1742-6596/1495/1/012012.

38. Abdullah, A.; Mohammed, A. Scanning Electron Microscopy (SEM): A Review. *Proc. 2018 Int. Conf. Hydraul. Pneum. - HERVEX* **2019**, 77–85.

39. Lu, J.; Li, Y.; Li, S.; Jiang, S.P. Self-Assembled Platinum Nanoparticles on Sulfonic Acid-Grafted Graphene as Effective Electrocatalysts for Methanol Oxidation in Direct Methanol Fuel Cells. *Sci. Rep.* **2016**, *6*, 1–12, doi:10.1038/srep21530.

40. Wang, Y.; Hu, M.; Ai, D.; Zhang, H.; Huang, Z.H.; Lv, R.; Kang, F. Sulfur-Doped Reduced Graphene Oxide for Enhanced Sodium Ion Pseudocapacitance. *Nanomaterials* **2019**, *9*, doi:10.3390/nano9050752.

41. Chen, Y.; Li, J.; Mei, T.; Hu, X.; Liu, D.; Wang, J.; Hao, M.; Li, J.; Wang, J.; Wang, X. Low-Temperature and One-Pot Synthesis of Sulfurized Graphene Nanosheets via in Situ Doping and Their Superior Electrocatalytic Activity for Oxygen Reduction Reaction. *J. Mater. Chem. A* **2014**, *2*, 20714–20722, doi:10.1039/c4ta04938a.

42. Li, Z.; Jiang, Y.; Wang, Z.; Wang, W.; Yuan, Y.; Wu, X.; Liu, X.; Li, M.; Dilpazir, S.; Zhang, G.; et al. Nitrogen-Rich Core-Shell Structured Particles Consisting of Carbonized Zeolitic Imidazolate Frameworks and Reduced Graphene Oxide for Amperometric Determination of Hydrogen Peroxide. *Microchim. Acta* **2018**, *185*, doi:10.1007/s00604-018-3032-y.

43. McCrory, C.C.L.; Jung, S.; Ferrer, I.M.; Chatman, S.M.; Peters, J.C.; Jaramillo, T.F. Benchmarking Hydrogen Evolving Reaction and Oxygen Evolving Reaction Electrocatalysts for Solar Water Splitting Devices. *J. Am. Chem. Soc.* **2015**, *137*, 4347–4357, doi:10.1021/ja510442p.

44. Feng, L.; Wang, R.; Shi, Y.; Wang, H.; Yang, J.; Zhu, J.; Chen, Y.; Yuan, N. Electrochemical Study of Hydrogen Peroxide Detection on MnO2 Micromaterials. *Int. J. Electrochem. Sci.* **2016**, *11*, 5962–5972, doi:10.20964/2016.07.42.

45. Navik, R.; Gai, Y.; Wang, W.; Zhao, Y. Curcumin-Assisted Ultrasound Exfoliation of Graphite to Graphene in Ethanol. *Ultrason. Sonochem.* **2018**, *48*, 96–102,

doi:10.1016/j.ultsonch.2018.05.010.

46. Fang, H.; Bian, H.; Zhang, H.; Wang, M.; Zhang, S.; He, L. Hierarchical Porous Nitrogen-Doped Carbon Nanosheets Derived from Zinc-Based BioMOF as Flexible Supercapacitor Electrode. *Appl. Surf. Sci.* **2023**, *614*, 156154, doi:10.1016/j.apsusc.2022.156154.

47. Kamyabi, M.A.; Mohammadian, H.; Jadali, S.; Moharramnezhad, M. Hydrothermal Syntheses of NiO−GO Nanocomposite on 3D Nickel Foam as a Support for Pt Nanoparticles and Its Superior Electrocatalytic Activity towards Methanol Oxidation. *Electroanalysis* **2019**, *31*, 1501–1510, doi:10.1002/elan.201800793.